Arabian Journal of Geosciences (2024) 17:250
https://doi.org/10.1007/s12517-024-12047-7

ORIGINAL PAPER

The Late Oligocene–Early Pleistocene paleoclimatic pattern in the northeastern Sahara, Sohag Basin, Egypt: evidence from lithofacies and pedogenic features

Tawfiq Mahran[1]

Received: 24 April 2024 / Accepted: 31 July 2024 / Published online: 19 August 2024

Abstract
The lithofacies and pedogenic features in the Late Oligocene–Early Pleistocene formations provide evidence of changing paleoclimate in the northeastern Sahara region. The strata of the Katkut Formation and the lower Member of the Madamud Formation consist predominantly of coarse and fine-grained siliciclastic lithofacies deposited by braided and sinuous streams that formed under the influence of humid paleoclimate during the Late Oligocene–Late Miocene time. Paleosol horizons with mature calcretes in the overlying upper member of the Madamud Formation suggest increasing aridity by the end of Late Miocene through Pliocene time. This trend of aridification continued during the Early Pleistocene lacustrine deposition of Issawia and Armant formations, as indicated by the predominance of palustrine carbonates displaying different pedogenic features. The climate change may have resulted from the southward movement of Asian monsoons and the uplifts of the Red Sea Mountain chains, as the African continent drifted northeastward. This paleoclimate transition generated variations in basin sedimentation rates that were controlled by base level and tectonics.

Keywords Lithofacies · Lacustrine · Palustrine · Calcrete · Paleoclimate · Sahara · Nile Valley

Introduction

The significance of Cenozoic continental deposits (fluvial and lacustrine-palustrine carbonates) has increased recently on a worldwide scale due to responses to climate change, which are essential to understanding the evolution of landscapes (Ramstein et al. 1997; Armenteros and Huerta 2006; Türkmen et al. 2007; Dupont-Nivet et al. 2007; Alçiçek and Jiménez-Moreno 2013; Cabaleri et al. 2013; Eronen et al. 2015; Gürel 2017). Additionally, the sedimentary features of pedogenic carbonates, calcretes, and paleosols are regarded as a paleoclimate archive (Tanner 2000; Alçiçek and Jiménez-Moreno 2013; Alonso-Zarza et al. 2011; Cabaleri et al. 2013).

The Late Cenozoic fluvio-lacustrine sedimentation in the northwestern Sahara (i.e., the entire region of north Africa) is influenced by paleoclimatic changes, particularly in the Chotts Basin of Tunisia and Algeria (Swezey 2009) and in the Ouarzazate Basin in Morocco (Boulton et al. 2019). However, paleoclimate changes of Late Cenozoic fluvio-lacustrine succession from the northeastern Sahara, which forms part of the southwest Mediterranean, are scantily documented. Thus, the importance of the current study has been utilized to interpret changes in the paleoclimatic regime between humid and more arid states of the examined succession in the Sohag basin (Fig. 1). This was documented from the presence and absence of calcrete-bearing paleosols and palustrine carbonates in the sedimentary succession. The non-calcareous paleosols that lack calcretes indicate that the climate was sub-humid to humid. In contrast, the predominance of groundwater calcretes in the calcareous paleosols indicates an increase in aridity. For example, Tanner and Lucas (2006) highlighted the transition from non-calcareous to calcareous paleosols as evidence of a change from wetter to drier climate conditions during the Late Triassic. In the study area, the Katkut Formation (Late Oligocene) and the overlying lower member of the Madamud Formation (Late Miocene) exhibit features suggesting deposition during humid conditions. Furthermore, features of the upper

Responsible Editor: Attila Ciner

✉ Tawfiq Mahran
mahranamh_9900@yahoo.com

[1] Geology Department, Faculty of Science, Sohag University, Sohag, Egypt

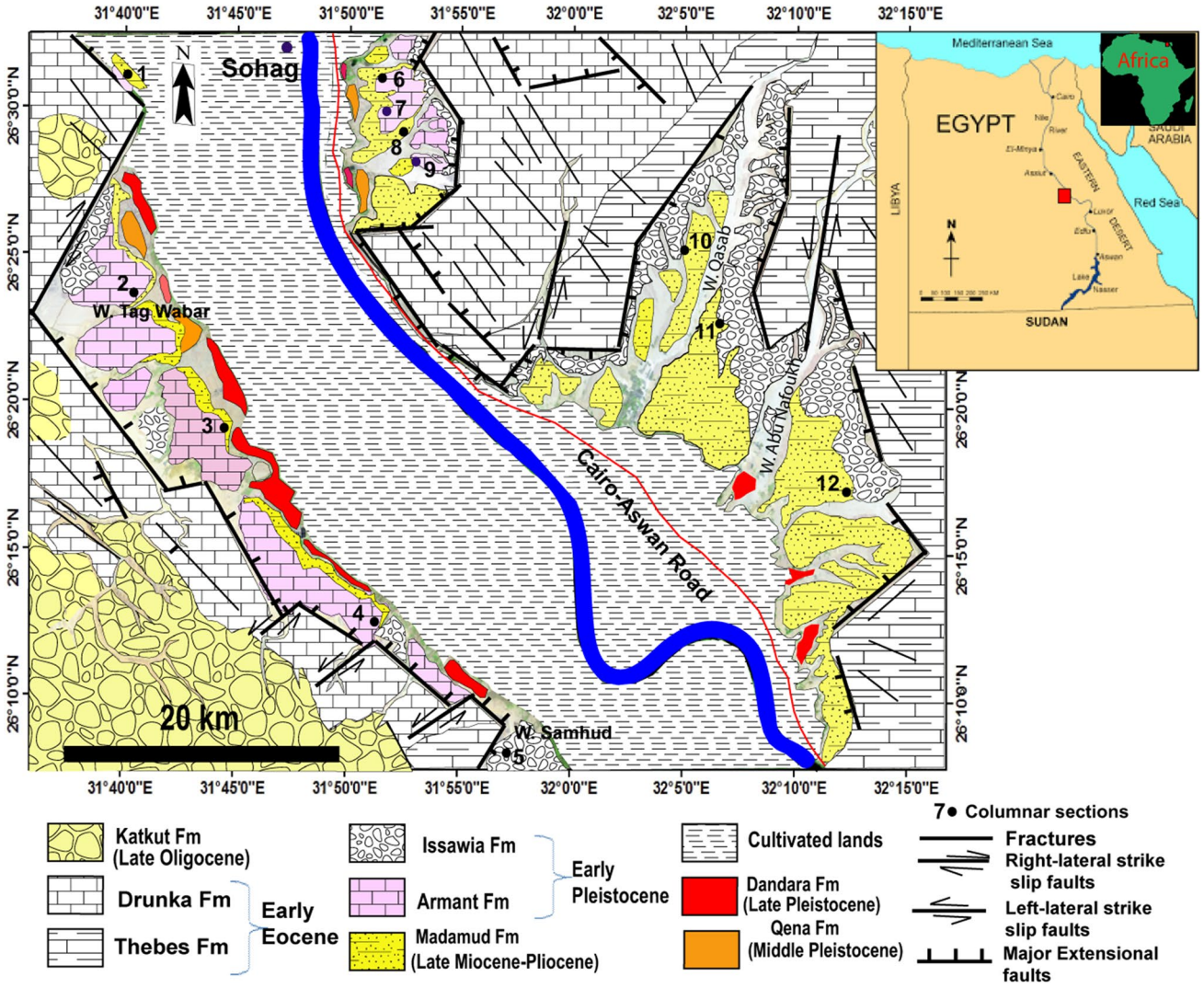

Fig. 1 Simplified geological map of the Sohag basin showing the distribution of Late Oligocene–Quaternary succession (modified after Mahran and Hassan 2023)

portion of the Madamud Formation (Pliocene) and the Issawia and Armant formations (Early Quaternary) show a shift towards dry paleoclimate (Mahran and Hassan 2023). Thus, the Late Oligocene–Early Quaternary succession provides valuable materials for the study of paleoclimate evolution in the northeastern Sahara. Previous studies of the Late Oligocene–Early Quaternary have mainly focused on the stratigraphy, mineralogy, and regional sedimentological characteristics (Said 1981; 1990; Bekir and Mahran 1992; Issawi and McCauley, 1993; Abu Seief 2015; El Shater et al. 2018; Mahran and Hassan 2023). However, the paleoclimate issue has not received enough attention. Therefore, the primary goal of this study is (1) to address the lithofacies architecture and the paleoenvironments and reconstruct a depositional model; (2) to discuss the lithologic variability and pedogenic features in view of paleoclimate and tectonic characteristics, and (3) to correlate them with the global paleoclimatic changes and the Sahara development throughout the Late Oligocene–Early Pleistocene. This will be employed through an integrated technique combining field and sedimentological characteristics.

The Sohag Basin: tectonic and stratigraphic setting

The Sohag Basin developed as a 30 km wide and 75 km long local graben with a NW–SE trend. It is bordered by two large rising plateaus composed of two distinct rock units: the Early Eocene Thebes and Drunka formations (Said 1990). The plateaus that encircle the basin are dissected by lineaments (fractures and normal faults) that generally trend NW, NNE, and ENE. The NW-striking faults that downthrow into the basin appear as straight

lengths that are both parallel to the basin's direction and defined by its escarpments (Fig. 1). According to Mahran and Hassan (2023), the NNE and ENE faults are cross-strike faults that are transverse to the basin axis. They are left- and right-lateral strike-slip faulting. The links between the NW extensional faults are frequently formed by faults with an ENE or NNE tendency. Straight wadi parts like Wadi Samhud, Wadi Tag El Wabar, and Wadi Abu Nafoukh are organized within these faults (Fig. 1). Similar NW-, ENE-, and NNE-striking faults have been described in the Beni Suef, Qena, and Wadi Kubbania basins (El Haddad 2007; Bosworth et al. 2008; Lansbery 2011; Abdelkhalek and Kley 2019; Abdelkhalek et al. 2020).

The general stratigraphic succession of the Sohag Basin includes six stratigraphic units which range from Late Oligocene to the Quaternary in age (Fig. 2a, b). Previous works (e.g., El Deftar et al. 1978; Said 1990; Issawi and Osman 2008; El Haddad 2014; Abu Seif 2015) provide the stratigraphic context, Nile phases, and age limits for this succession. The Katkut Formation (Late Oligocene) corresponds to the pre-Eonile Phase and consists of 30 m of reddish brown

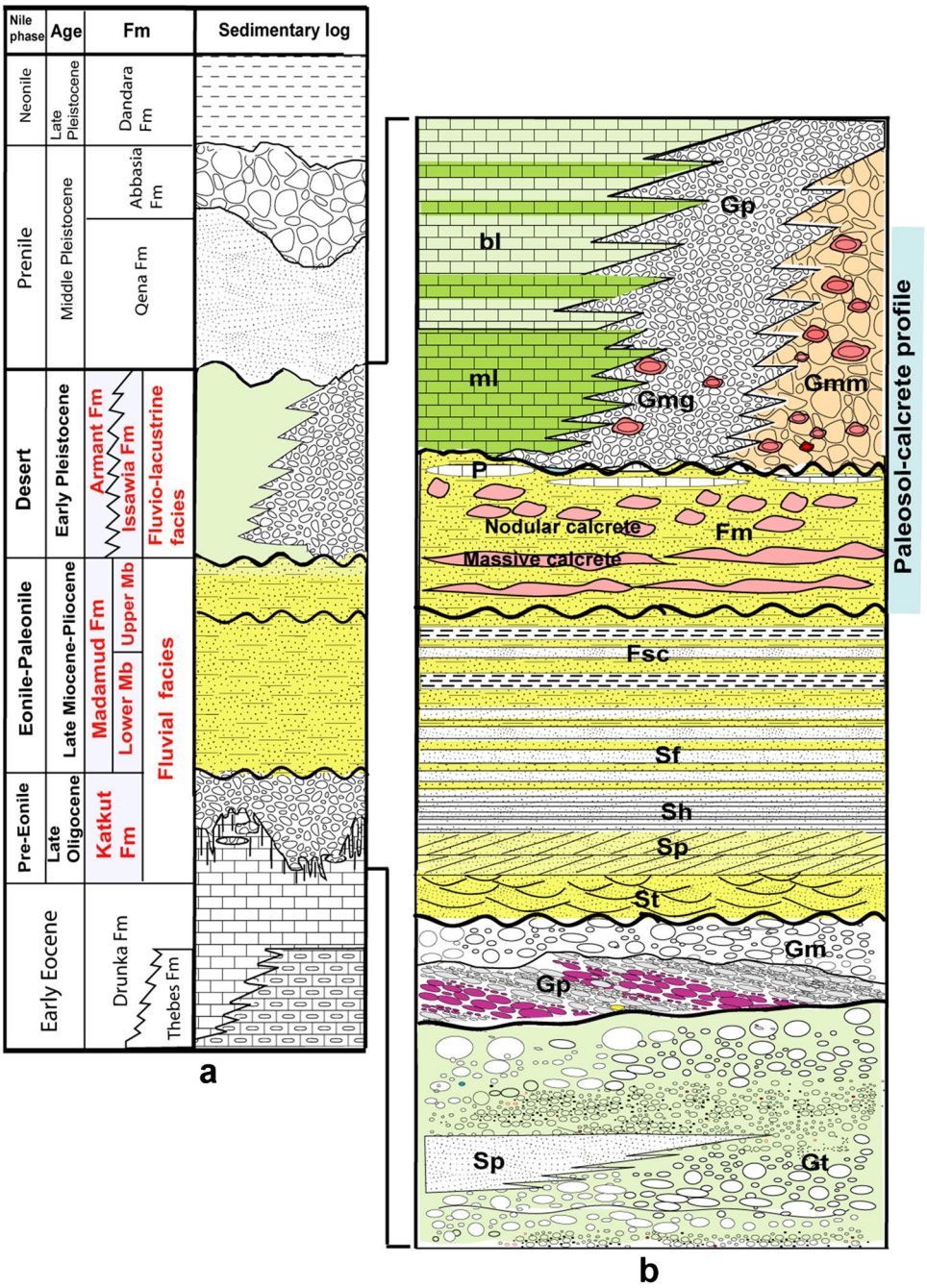

Fig. 2 **a** Generalized lithostratigraphy of the Late Oligocene and Quaternary succession cropping out in the Sohag basin (data after El Ayyat 1989; El Hinnawi et al. 1978; Said 1981, 1990; El Haddad 2014; Abu Seif 2015 and present study). **b** Details of studied Late Oligocene, Late Miocene, Pliocene, and Early Pleistocene succession showing the distribution of lithofacies

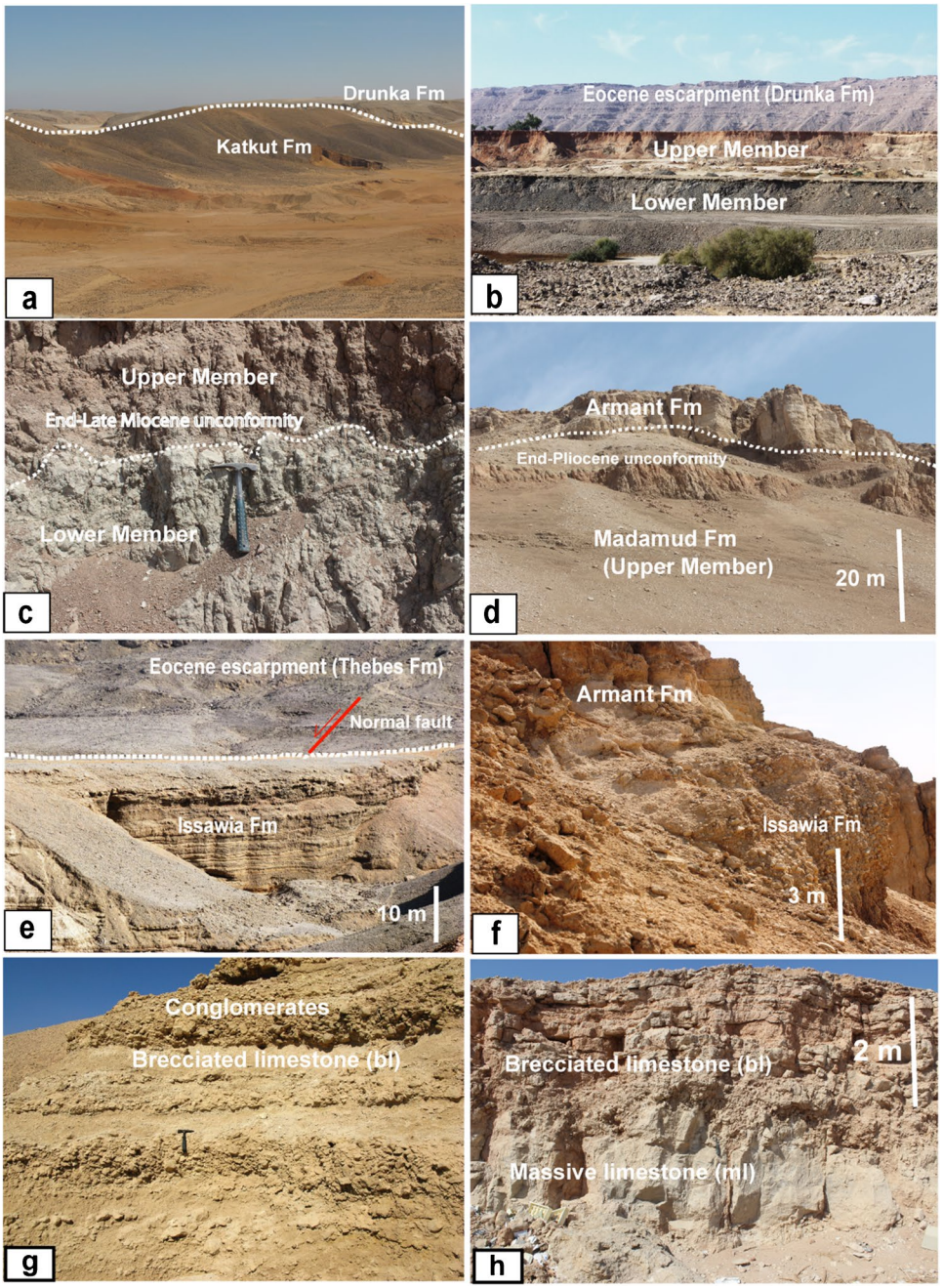

Fig. 3 **a** Field view showing the Katkut Formation unconformably overlying the Drunka Formation. **b** The Armant Formation unconformably overlies the Madamud Formation. **c** A panoramic view of the grey and reddish brown facies of the Madamud Formation is near the Eocene escarpment. **d** A close-up view showing the upper member of Madamud Formation unconformably overlies the lower Member. **e** Cliff exposure of stratified conglomerates of the Issawia Formation cropping out at footslopes of Eocene escarpment. **f** Conglomerate tongue of the Issawia Formation overlain by carbonates of the Armant Formation. **g** Stratified conglomerates (Issawia Formation) interbedded with brecciated limestone (Armant Fm). **h** Upward gradual transition from massive limestone to brecciated limestone of the Armant Formation

coarse siliciclastic deposits (Fig. 3a) that are unconformably overlying the Lower Eocene Drunka Formation (El Deftar et al. 1978; Swezey 2009) and unconformably overlain by the Madamud Formation. The overlying Madamud Formation (Late Miocene–Pliocene) reaches a maximum thickness of 50 m and corresponds to the Eonile and Paleonile phases. It is subdivided into a lower member consisting of sandstone grading upwards into grey claystone and mudstone, and an upper member is dominated by mudstone and calcrete deposits (Fig. 3b, c). The Issawia and Armant formations (Early Pleistocene) rest unconformably on the underlying Madamud Formation (Said 1990; El Haddad 2014). These units are about 30 m thick and principally made up of breccias and conglomerates (Issawia Formation, Fig. 3d, e) that interfinger and grade laterally into massive and brecciated lacustrine carbonates (Armant Formation, Fig. 3f–h), both of which are related to the Desert phase of Said (1981, 1990). The overlying Abbasia and Qena formations (Middle Pleistocene), which belong to the Prenile phase, consist primarily of sandstones and conglomerates. The Late Pleistocene Dandara Formation, which is part of the Neonile phase and represents the basin's final filling, is composed of claystone

deposits. This investigation focuses on the Late Oligocene, Late Miocene, Pliocene, and Early Pleistocene deposits that correspond to the Katkut, Madamud, Issawia, and Armant formations.

Material and methods

A detailed geological map was created (Fig. 1) and eleven well-exposed stratigraphic columnar sections were constructed. Five of the sections were located in the west of the Sohag Basin between Latitudes 26° 09′ and 26° 26′ N and Longitude 31° 39′ and 31° 50′ E. Six of the sections were located in the east between Latitudes 26° 17′ and 26° 31′ N and Longitude 31° 50′ and 32° 14′ E. These sections were regionally correlated to show the overall variation from fluvial to mixed fluvio-lacustrine limestone. Based on grain size and dominant sedimentary features, the major lithofacies types are recognized and modified in accordance with the lithofacies classifications suggested by Miall (1978, 1996). The corresponding depositional environment for each lithofacies is interpreted. Depositional model is made based on the defined facies associations and their spatial distribution. To study the fabric and composition of the calcretes and limestones, petrographical studies were carried out on fifty representative thin sections in conglomerates, breccias, calcretes, and lacustrine-palustrine limestones. The impact of lithofacies changes and pedogenic characteristics on the development of paleoclimate in Late Oligocene–Early Pleistocene times was discussed and compared with surrounding situations from the Mediterranean, northwestern Sahara regions as well as the global paleoclimate.

Results

On the basis of lithology and sedimentologic features, sixteen lithofacies have been identified within the studied successions. These lithofacies are organized into two main facies associations; the fluvial and the fluvio-lacustrine. The detailed descriptions and interpretations of these associations are given in Tables 1, 2, 3, and 4, and a summary is provided in the following paragraphs. The associated calcrete and paleosol profiles are also discussed.

Fluvial facies association

The fluvial association constitutes the Katkut and Madamud formations and comprises eleven lithofacies types. Four lithofacies (*Gt*, *Sp*, *Gp*, and *Gm*) represent the Katkut Formation (Fig. 4). Five lithofacies types (*St*, *Sp*, *Sh*, *Sf*, and *Fsc*) make up the lower member of the Madamud Formation. The upper member includes two lithofacies types (*Fm* and *p*). These lithofacies are identified and interpreted as follows:

Lithofacies Gt: massive or crudely bedded conglomerate

Lithofacies *Gt* is the most prevalent lithofacies type close to the base of the Katkut Formation. Conglomerate dominates this lithofacies, which is primarily made up of gravel-sized carbonate and chert. Also, quartz pebbles are predominant. *Gt* has broad small sandstone lenses that form a wedge-like geometry (Fig. 5a). Lithofacies *Gt* infills subsiding karstified depocenters (Mahran and Hassan 2019). The majority of these lithofacies are fining upwards, with some channel-like bodies. The conglomerates are rounded, imbricated, and clast-supported fabrics that are bimodal, immature, and extremely coarse in texture (Fig. 5b). Paleosol horizons within conglomerate deposits are common. Laterally, the bedded gravels give way to a thick cross-bedded sand with gravel lobes.

Interpretation

The massive conglomerate bars and channel-fill sands of lithofacies *Gt* are interpreted as braided channel deposits similar to those reported by other writers in different settings (Miall 1996; Braulta et al. 2004; Kjær et al. 2004; Soreghan et al. 2009). This interpretation implies high levels of water and strong gravel transportation as a result of a large sediment supply (Miall 2010). These rapid flow conditions are demonstrated by the coarser pebble-to-cobble size clasts, clast-support, imbricated fabrics, and scouring. The presence of rounder conglomerate clasts may imply periodic abrasion as well as long-distance transportation. The presence of silicified limestone and chert clasts, as well as quartz pebbles, suggests that they are sourced from Lower Eocene and Mesozoic rocks. The presence of paleosol horizons within conglomerate deposits may indicate the discontinuous nature of braided deposition (Abdul Aziz et al. 2003).

Lithofacies Sp: planar cross-stratified sandstone

Sandstones with medium to coarse-grained and moderately well-sorting and gravel lenses make up the majority of these lithofacies and are enriched with root traces that grade laterally into the bedded conglomerates *Gt*. The sandstone is mainly quartz, with a few minor traces of carbonate rock fragments. This lithofacies is dominated by stories with vertically stacked sand that show large-scale planar cross-bedding sets that are tabular and have a fining upward trend. The tabular foresets show a regional paleocurrent flowing northward. An erosional lower limit can be seen on individual foresets. Lateritic ferruginous paleosols (2–5 m thick) and considerable iron impregnation in the groundmass, as

Table 1 Summary of list of the lithofacies types in the Katkut Formation

Lithofacies (code)	*Description*	*Interpretation*
Gt: massive or crudely bedded conglomerate	Grey colour, clast-supported, well-sorted, imbricated, erosive base, crude bedding, gravel up to 25–30 cm (total thickness 5–15 m). Laterally, the bedded gravels grade to a thick cross-bedded sand and gravel layer with gravel lobes	It is deposited as gravel bars in braided rivers under high-velocity flow and high water levels
Sp: planar cross-bedded sandstone	Grey colour, overlying gradationally the *Gmm* or acute the erosive scouring. Pebble- to cobble-grade clasts are subrounded to, reddish brown, poorly sorted with a mixture of mud and sand. A total thickness of approximately 8 m. Paleocurrent patterns from some imbricated clasts indicate transverse transport, towards the axis of the basin	It is deposited in an alluvial fan environment dominated by debris flows
Gp: planar cross-stratified conglomerate	Conglomerates that range in colour from reddish brown to grey have pebble- to cobble-grade clasts and are subangular to subrounded. Total thickness (20 m). It is separated from the underlying lithofacies *Gmg* by an unconformity with an irregular erosional surface. Low-angle planar cross-bedded conglomerates are occasionally associated with planar, cross-bedded sandstone. The thicknesses of the cross-bed sets and their cosets are 0.5 to 1 m and up to 5 m, respectively	It is produced by the migration of point bars within braided channels
Gm: stratified conglomerate	Reddish brown colour, parallel bedding. The clast was supported by a matrix of sandstone. The largest clast is 30 cm. Well-rounded to subrounded, commonly imbricated. Total thickness (3–5 m). Ferruginous paleosols and crusts are predominant	It was presumably deposited in braided channels and developed by vertical accumulation on longitudinal bars

Table 2 Summary of the list of the lithofacies types in the Madamud Formation

Lithofacies (code)	*Description*	*Interpretation*
St: trough cross-bedded sandstone	Sandstone lithofacies, consisting primarily of quartz and lithic fragments, is yellow in colour, coarse to medium-grained, pebbly, and poorly to moderately sorted. The total thickness can be up to 4 m. A wide paleocurrent that flows northward, a trough cross-stratification that is 10–40 cm thick, upward-fining sets, and a maximum dip angle of about 30°	It is deposited in low-sinuous river channel during conditions of high velocity
Sp: planar cross-bedded sandstone	Brownish quartz arenite and subarkose sandstone, coarse to fine-grained, moderately to well-sorted, occasionally poorly sorted. The thickness ranges from 5 to 8 m. Planer cross-bedding with upward fining sets. High-angle (20–30°) foresets predominate at the base, which grade upward to low-angle foresets (10–15°)	It is deposited in high-sinuous fluvial channels that have deep and shallow conditions
Sh: horizontal sandstone	Fine- to medium-grained yellow sandstones with feldspathic and occasionally arenite in composition. Its thickness is about 2 to 4 m, with a lateral extension of hundreds of metres. Geometry ranging from sheet-like to tabular. Lamination that is primarily horizontal and parallel (1–2 cm), with low-angle cross lamination. Root burrows and rhizoliths occur sporadically	As a result of the medium and low flow regimes, it is accumulated as in-channel deposits
Fi: laminated sandstone–siltstone	Alternating with siltstone and sandstone showed yellow and grey colour. Sandstones are fine to very fine-grained and moderately to well-sorted. Total thickness varies from 2 to 10 m. Horizontal lamination and occasionally cross-lamination in places. It contains rhizoliths and is locally mottled	It is deposited in crevasse splays and levee areas on floodplains during varying food stages
Sf: interbedded sandstone–siltstone–claystone	Grey fine sandstone, siltstone, and claystone constitute tabular-bed geometry. Total thickness ranges from 2 to 8 m. The lithofacies are often gradational, and the top contacts are either engraved by massive calcrete or paleosol. Slickenside desiccation cracks are common	It is deposited in standing water bodies during various flood stages before being deposited in an overbank, floodplain environment
Fm: siltstone, claystone, and massive mudstone	Brown to reddish brown siltstone, claystone, and massive mudstone (up to 8 m thick). The length of the beds is in the tens of metres. Mudstones of varying sizes have cracks that are filled with a greyish-white calcium carbonate material. Calcretes formed in the upper parts of lithofacies, with colour changes ranging from light grey to yellowish white. The lower calcrete has siliciclastic intercalations and is massive and cyclic. The top crust has a nodular texture. The vertically extending nodules exhibit desiccation fractures and mottling	It is mostly deposited in the overbank and distal areas from suspension. floodplains, abandoned channels with calcretization processes
P: *pedogenic limestone*	Red-mottled muddy limestone; the range of thickness is 0.4 to 1 m. Evidence of palustrine features can be seen in the beds. Pseudomicrokarsts, or cavities, are also common. They are elongated, up to 4.0 cm long and up to 1.0 cm high. Sparry calcite makes up the majority of their lining	It is deposited in ponds with shallow water that have grown on flood plains, where it is modified by subaerial exposure

Table 3 Summary of the list of the lithofacies types in the Issawia Formation

Lithofacies (code)	*Description*	*Interpretation*
Gmm: clast-supported, massive gravels and, breccias	Aggradationally grey to reddish brown colour stacked, crudely bedded breccias, gravels composed of disorganized limestone, and chert clasts that are typically poorly sorted and comprise clast-supported fabrics, alternating with facies *Gmg*. Thickness (10–20). Recrystallization and streaking processes are visible in clasts. Clasts are cemented by sand and silt-sized materials	It is formed due to the reactivation of fault movements (i.e., fault breccias)
Gmg: matrix-supported conglomerates	Grey colour, graded with the *Gmm* or occasionally with erosive scouring. Pebble- to cobble-grade clasts are subrounded to subangular, reddish brown, poorly sorted mixtures of mud and sand matrix. They are supported by the matrix. A total thickness of approximately 10 m. Subrounded to rounded and some are subangular; all are embedded in a coarse calcite and fine-grained sand matrix. Paleocurrent patterns from some imbricated clasts indicate transverse transport, towards the axis of the basin	It is deposited in an alluvial fan environment dominated by debris flows
Gp: planar cross-stratified conglomerates	Grey to reddish brown, conglomerates of pebble- to cobble-grade clasts that are subrounded to subangular, reddish brown, and poorly sorted mixtures of mud and sand matrix. Total thickness (5–10 m). It is separated from the underlying lithofacies *Gmg* by an irregular erosional surface. Low-angle planar cross-bedded conglomerates that are occasionally occurring with planar, cross-stratified sandstone. The thickness of the cross-bed sets and their cosets range from 0.5 to 1 and up to 5 m, respectively	It is created by the movement of linguoid, transverse, or point bars within a braided system or a gravel-bed meandering stream

Table 4 Summary of the list of the lithofacies types in the Armant Formation

Lithofacies (code)	*Description*	*Interpretation*
ML: massive limestone	Dense, homogeneous without lamination, whitish yellow, bedded, fossiliferous, thicker at the base (up to 1 m), and tends to thin out higher by up to 0.4 m. Commonly grade vertically and laterally into the brecciated lithofacies *BL*. Petrographically, they are micrites with mudstone to wackestone textures that have gastropods, charophytes, and ostracods in them. The beds are affected by shrinkage cracks	It is deposited in relatively deep, low-energy lake water conditions with an increased sedimentation rate
BL: brecciated limestone	Yellowish white, porous, and composed of micrite and microsparite; it increases in thickness towards the basin margins, from 5 to 10 m, and is thin-bedded in individual beds (up to 0.5 m thick). It exhibits a variety of pedogenic features and is composed of three fabrics: rhizolitic, intraclastic, clotted-peloidal, brecciated, and nodular. Root traces are frequent, particularly near the tops of the beds. Fissures and circumgranular cracks are frequent, and sparry calcite may occasionally fill these structures as well as vugs, channels, fenestrae, and pseudomicrokarst cavities	It is deposited in a shallow palustrine environment under multiple conditions of prolonged subaerial exposure. Strong rhizoliths and vertical cracks that taper downhill are signs of a low-gradient lake margin setting

well as Fe–Mn nodules and concretions, mark the top of this lithofacies.

Interpretation

Based on the erosional lower boundary and fining-upward tendency, the lithofacies *Sp* is interpreted as channelization deposits. This interpretation is further supported by the abundance of root traces close to the top and the existence of unidirectional flow. Sandstones with an abundance of gravel lenses suggest intermittent, high-energy depositional conditions. The multistory deposits of sand that are vertically stacked interpret that multiple ancient rivers played an important role in aggradation and transport of materials during earlier pluvial periods (Abdelkareem et al. 2012). The presence of red paleosols terminated this lithofacies indicates subaerial exposures and weathering of the carbonate-dominated conglomerates.

Lithofacies Gp: planar cross-bedded conglomerate

The overall thickness of lithofacies *Gp* is approximately 20 m. This lithofacies frequently truncates the underlying lithofacies *Sp* of the channel deposits as well as the paleosols. The *Gp* is composed of interbedded conglomerates and conglomeratic sandstones. This lithofacies is notable for its large-scale foresets, which can be found in cliffs up to 10 m high. The stratification of the foreset beds ranges from 20 to 50 cm in thickness and has a 30° average dip that gradually decreases to 15°. The thickness of the set varies from 5 to 30 cm. Paleocurrent directions in lithofacies *Gp* that flow mainly northward are compatible with the underlying planar cross-bedded sandstone. The conglomerate beds of lithofacies *Gp* are clast-supported and consist of mixed silicified limestone, chert, and quartz. Clasts range in size from 5 to 15 cm and are well- to sub-rounded.

Interpretation

This lithofacies is believed to have developed as a result of linguoid bars or point bars migrating in braided systems or gravel-bed meandering streams (Miall 1977). An irregular erosional surface separates the foreset gravels from the overlying lithofacies, indicating that the majority of the lower lithofacies emerged and were eroded prior to the formation of the above gravels. The increase of foreset beds at the base of this lithofacies indicates the deposition developed upon a high gradient basin margin.

Lithofacies Gm: stratified conglomerate

This lithofacies terminates the Katkut Formation. Lithofacies *Gm* commonly truncates the lithofacies *Gp* of the channel deposits across erosion surfaces. The upper and lower bedding borders are sharp to slightly scoured and exhibit sheet geometries. This lithofacies occurs as sheet-like conglomerate bodies. This lithofacies is red in colour and exhibits parallel bedding due to distinct clast-size segregation and pebbles oriented parallel to their longitudinal axes. The greatest clast size varies from 10 to 30 cm, and

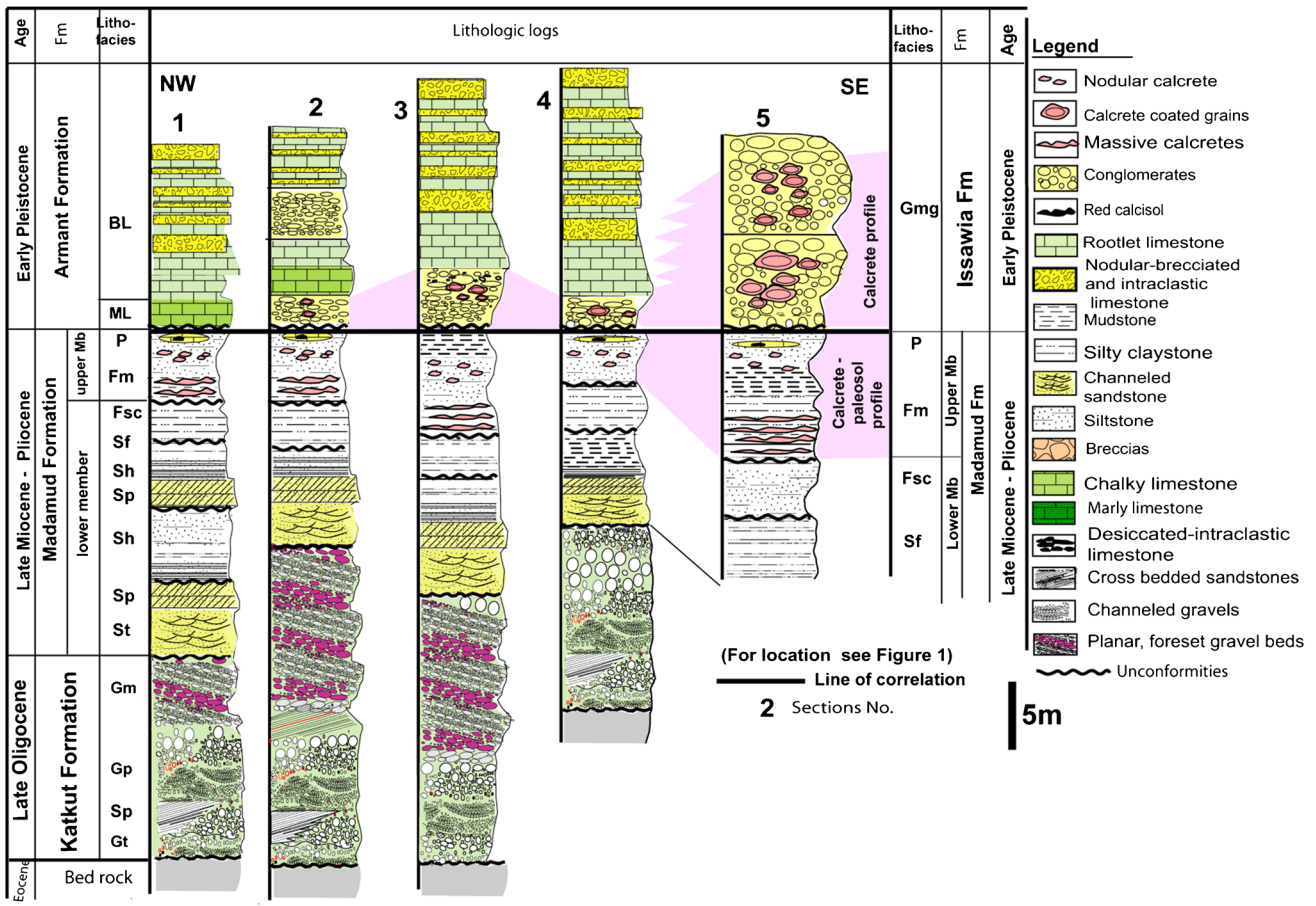

Fig. 4 NW–SE stratigraphic log correlation showing the along-western margin lithofacies changes of the fluvial lithofacies of the Madamud Formation and mixed fluvio-lacustrine lithofacies (Issawia and Armant formations). Note the vertical changes of the calcrete profile from the massive at the base into the nodular type in its upper part. The calcrete-coated grains dominate the Issawia Formation. Datum is on top of the Madamud Formation

it is clast-supported with a sandy matrix, and some have an imbricated fabric. The clasts appear to be more sorted, well-rounded, and subrounded in texture. Large blocks of the underlying Drunka Formation that attain 1 m in diameter are found. Lateritic ferruginous paleosols (0.5 m thick) and considerable iron impregnation in the groundmass.

Interpretation

This lithofacies is similar to the *Gm* lithofacies described by Miall (1996). The sheet-like conglomerates were believed to have formed by vertical accumulation on longitudinal bars that were deposited in small, low-sinuosity channels (Miall 1996). Similar lithofacies have been previously observed in sheet food deposits (Blair and McPherson 1994; Türkmen et al. 2007). Clasts of Fossiliferous limestone with minor cherty limestone predominate the topmost of this lithofacies, suggesting streams originating from the surrounding Lower Eocene strata. The reddish colour of this lithofacies is indicative of oxidizing conditions and deep groundwater table (Tuner 1980).

Lithofacies St: trough cross-bedded sandstone

This lithofacies has developed on each side of the basin and expands hundreds of metres laterally and becomes thicker towards the centre of the basin. The thickness of the set ranges from 5 to 15 cm. Lithofacies *St* consists of brown to yellow, coarse-grained to gravelly, and poorly sorted sandstone. The sand grains are coarse to medium size, rounded, moderate to poorly sorted with pebbles of quartz, and sometimes have compositions that are both feldspathic and quartz arenite. This lithofacies is only present in the lowest and middle parts of the Madamud Formation displaying fining-upward cycles. The troughs are formed by a curve set with an angle of dip. Poorly sorted lags are frequently associated with the bases of troughs. Sediments of this lithofacies indicate a dominant paleoflow with a northward and northeasterly direction. The lithofacies *St* deposits can be

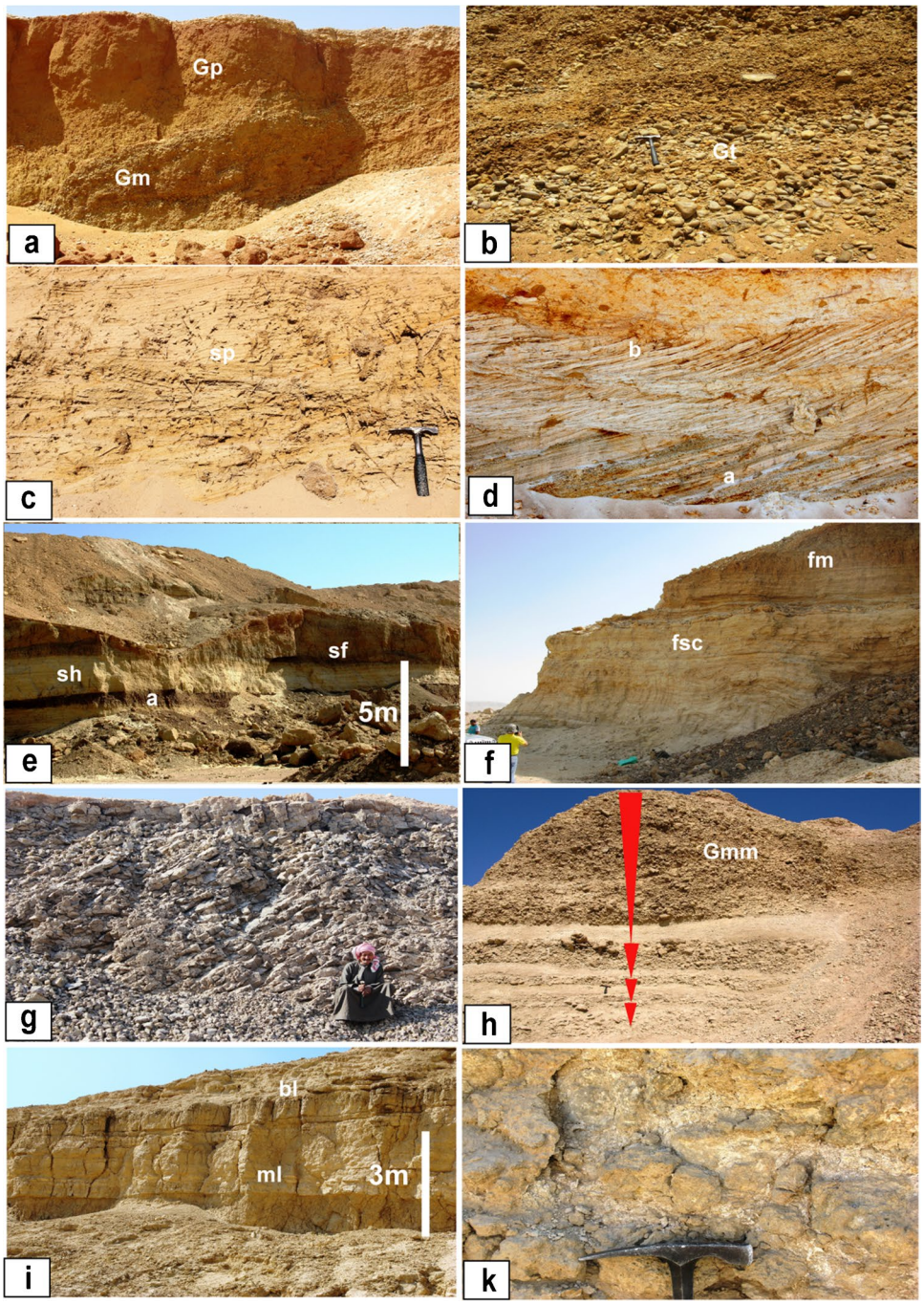

Fig. 5 **a** Planar cross-bedded conglomerate (*Gm*) overlain by a stratified conglomerate (*Gp*), Katkut Formation. **b** Crudely bedded conglomerates (*Gt*) are characterized by fining-upward cycles. **c** Cross-bedded sandstone interrupted by plant roots plant roots (*Sp*). **d** Multi-story planar cross-bedded sandstones (*Sp*). Note that the planar cross-bedding displays a high angle of dip at the basal part (a), passing upwards into small-scale cross-bedding with low angles of dip (b), **e** Horizontal sandstone (*Sh*) overlain by laminated sandstone–siltstone lithofacies (*Sf*). Note that mottled clay lenses (a) filling troughs within sandstone deposits. **f** Interbedded sandstone, siltstone, and claystone (*Fsc*) unconformably overlain by massive siltstone, claystone, and mudstone (*Fm*). Note the highly deformed cross-bedded sandstone at the base of the photo. **g** Slickenside desiccation cracks in lithofacies *Fsc*. **h** Crude-bedded conglomerates (*Gmm*) are characterized by coarsening-upward cycles. Note the interbedded brecciated limestone near the top. **i** Massive and brecciated limestones (*ML* and *BL*). Note that the massive limestone (*Ml*) gradually passes upward into a brecciated limestone (*BL*). **k** A close-up view of brecciated and nodular fabrics of brecciated limestone

distinguished by the presence of downward-branching plant roots (Fig. 5c). The troughs in this lithofacies are filled by mottled clay lenses ranging in thickness from 0.5 to 1 m.

Interpretation

The lithofacies *St* is considered low-sinuosity fluvial channel deposits due to the nature of stacking patterns of the well-developed trough cross-bedded sandstone with erosive-bases and normal grading during high-velocity conditions (Paula-Freitas 2010). It has been suggested that the clay lenses are mud plugs. They have filled depressions that were made when the flood events slowed down and suspended silt and clay deposits were abundant.

Lithofacies Sp: planar cross-bedded sandstone

This lithofacies occurs overlying cross-bedded sandstone *St*. This lithofacies consists of brown to yellow to brown-coloured, coarse-to-medium-grained, moderately to well-sorted

sandstone. This sandstone is composed mainly of quartz, with a little amount of feldspar and rock fragments. This lithofacies consists of large tabular beds with planar cross-bedding sets that are typically less than 0.5 m thick (Fig. 5d). Quartz grains and pebbles can be found at the base of many set boundaries. In the lithofacies *Sp*, low-angle forests (10–15°) are less frequent than high-angle forests (20–30°). The paleocurrent measurements of cross-bedded sandstone reveal a northeastern to northern trend. The top of this lithofacies is composed of distinct fining-upward cross-beds with synsedimentary deformational characteristics, such as slumping and distorted folds.

Interpretation

This lithofacies exhibits planar cross-bedding transitions with a high angle of dip at the top and a small-scale cross-bedding with a low angle of dip at the bottom. This demonstrates that the upper part shows deposition in the shallow parts of the river channels (Miall 1996) whereas the basal portion suggests deposition in their deeper parts (Jo and Chough 2001). It has been suggested that the clay lenses are mud plugs. These are filled depressions formed when high-energy floods decreased and suspended silt and clay deposits were present. The rounded shapes of the quartz pebbles and sand grains indicate that the sediments underwent extensive transportation. Their origin, presumably from a source of Nubian sandstone in southern Egypt, is consistent with the tabular foresets' northward inclination, suggesting regional northward transportation. The deformational structures (slump and contorted folds) may indicate seismic activity caused by extensional movement.

Lithofacies Sh: horizontal sandstone

This lithofacies constitutes most of the studied sections of the Madmud Formation. Sheet-like to tabular geometry characterizes the lithofacies *Sh*. Beds typically comprise planar, cross-bedded sandstone, and flat bases with the underlying lithofacies *Sp*. The sedimentary features of this lithofacies that have been observed commonly are parallel laminations (1–2 cm thick, Fig. 5e). The lithofacies *Sh* sediments are fine- to medium-grained yellow sandstones. The majority of the sandstone has moderately to poorly sorted feldspar and quartz grains and is sub-angular to sub-rounded. Local vertical roots have bioturbated this lithofacies.

Interpretation

According to Miall (1996) and Javidan et al. (2015), the sheet-like to tabular fine-to-medium-grained lithofacies point to deposition as in-channel deposits as a result of waning during the traction-suspension process during flood events (Ghazi and Mountney 2010). Throughout traction mechanisms, medium-grained deposits may result in parallel lamination (Boggs 2006, 2009; Khalifa and Catuneanu 2008). Common biotubations provide further evidence of the fluvial plain's high plant cover, low rates of sedimentation, and quiet flowing conditions (Abdelfattah 2021).

Lithofacies Sf: laminated sandstone–siltstone

This lithofacies is distinguished by laminated, fine-grained grey and brown siltstone and sandstone, and generally, its lower contact is gradational with lithofacies *Sh*. The sandstone interbeds are sometimes channelized but very frequently sheet-type. The beds extend laterally as sheet-like geometry. The main primary structures that characterized this lithofacies are parallel lamination and small-scale cross-lamination. Usually, the basal and top boundaries are sharp. The *Sf* lithofacies is usually mottled and contains mature paleosol horizons that show rhizoliths, desiccation cracks, and nodular calcrete.

Interpretation

This lithofacies represents low-energy deposits that formed on floodplains in levee and crevasse splay zones during various floods (Sahraeyan and Bahrami 2012; Sahraeyan 2013). Despite channelized flows being found near the main channel, unconfined flows associated with crevasse splays are likely to have contributed to the deposition of the sheet-type sandstone (Kraus and Aslan 1999). The intercalation of fine-grained sand with the lithofacies *Sf* could indicate sudden changes in the flood regime or high-energy sheet floods into low-energy environments (Olsen 1988).

Lithofacies Fsc: interbedded sandstone–siltstone–claystone

Sediments of lithofacies *Fsc* are composed of sandstone, siltstone, and claystone which form a tabular-bed geometry. They extend laterally across hundreds of kilometres (Fig. 5f). The basal contact of this lithofacies is occasionally gradational with lithofacies *Sf*. The higher contacts of this lithofacies are either imprinted by massive calcrete and paleosols or truncated by erosive surfaces or sharp contacts with the overlying lithofacies *Fm*. This lithofacies frequently has surfaces with slickensides (Fig. 5g).

Interpretation

This lithofacies is thought to represent deposition from suspension in remaining water bodies throughout various flood levels in an overbank floodplain environment. (Türkmen et al. 2007; Bourquin et al. 2010). It is thought that

clay cracking, swelling, and shrinking during the drying and wetting cycle causes slickenside surfaces (Retallack and Alonso-Zarza 1998; Retallack 2001).

Lithofacies Fm: massive siltstone, claystone, and mudstone

This lithofacies dominates the upper member of the Madamud Formation and is composed mainly of red and brown siltstone, claystone, and mudstone. Sandstone lenses are commonly sheet-type but can also be channeled in some places. The basal contact of this lithofacies is characterized by an unconformity surface, which can be traced in most of the studied sections. Kaolinite mineral is the main composition of this lithofacies. Mud cracks and red-coloured mottling characterize this lithofacies. The *Fm* include widespread macroscopic paleopedogenic features (calcrete nodules and paleosols). The lower part of this lithofacies is dominated by cyclic nodules and massive calcretes and siltstones. Upward, nodular calcretes are the most common type.

Interpretation

Based on the grain sizes and sedimentary structures, the deposition of such lithofacies took place in an overbank environment (Ghazi and Mountney 2010; Sahraeyan 2013). The presence of red-coloured mottling in the claystone associated with fewer preserved sedimentary structures and blocky and platy beds documents flood plain deposition (Scherer et al 2015), providing evidence of soil formation (Alonso-Zarza 2003) and suggesting well-drained floodplains during the processes of oxidation and soil formation (Retlallack 2008). The relatively high kaolinite composition of the deposits supports the well-drained environment (Driese and Ober 2005; Sheldon and Tabor 2009). It is believed that the lenticular sands are crevasse deposits that developed during isolated events of floods.

Lithofacies P: pedogenic limestone.

This lithofacies is recorded within the upper member of the Madamud Formation (Fig. 6). It appears as limestone lenses which fill small troughs that sharply contact the surrounding lithofacies. The limestone in this lithofacies is distinguished by pseudo-microkarst cavities and polygonal desiccation cracks. They are typically elongated, up to 3 cm long and 1 cm tall, and lined with sparry calcite. Under a microscope, this limestone is identified as biomicrite wackestone with rare detrital quartz grains. It consists of skeletal components scattered throughout the micrite matrix.

Interpretation

This lithofacies is interpreted as palustrine deposits, accumulating in ponded water, that were caused by vertical aggradation of floodplains during low terrigenous sedimentation (Wright 1999; Pla-Pueyo et al. 2009), similar to those described by Freytet and Plaziat (1982) in the Cretaceous-Tertiary sequences of southern France. The polygonal cracks are thought to be desiccation cracks that formed during times of low levels of water. The absence of detrital grains in this lithofacies indicates that groundwater was the main source of water.

Fluvio-lacustrine facies association

This facies association represents the Issawia and Armant formations and comprises five lithofacies types: four lithofacies (*Gmm*, *Gmg*, and *Gp*) characterize the Issawia Formation and two lithofacies (*ML* and *BL*) for the Armant Formation. These lithofacies are identified and interpreted in the following:

Lithofacies Gmm: clast-supported, massive gravels, and breccias

Sediments of this lithofacies are characterized by a limited geographic distribution, and it situated close to the fault-bounded eastern and western scarps in the basin's peripheral area. It is a scree deposit belt situated near to an escarpment. It commonly unconformably overlies siltstone and massive clay of lithofacies *Fm*. *Gmm* lithofacies are aggradationally stacked, crudely bedded breccias and gravels composed of disorganized limestone and chert clasts that are typically poorly sorted and comprise clast-supported fabrics. The clasts are of various sizes, ranging from 0.2 to 1 m. The matrix consists mainly of coarse calcite and fine-grained silt and sand. Large fractures and dissolution channels are occasionally observed, together with coarse calcite crystals and red calcisoil.

Interpretation

Based on the crude-bedding and extremely angular clasts, talus aprons and scree deposits were the original sources of the clasts of the lithofacies *Gmm*. This lithofacies was probably formed from cracked bedrock and later deposition as colluvial debris on steep slopes because of the predominance of monomictic composition and the local provenance of the breccia clasts. Additional proof that colluvial debris was deposited comes from the severely disorganized fabric of clasts and the local inverse grading of several breccia beds

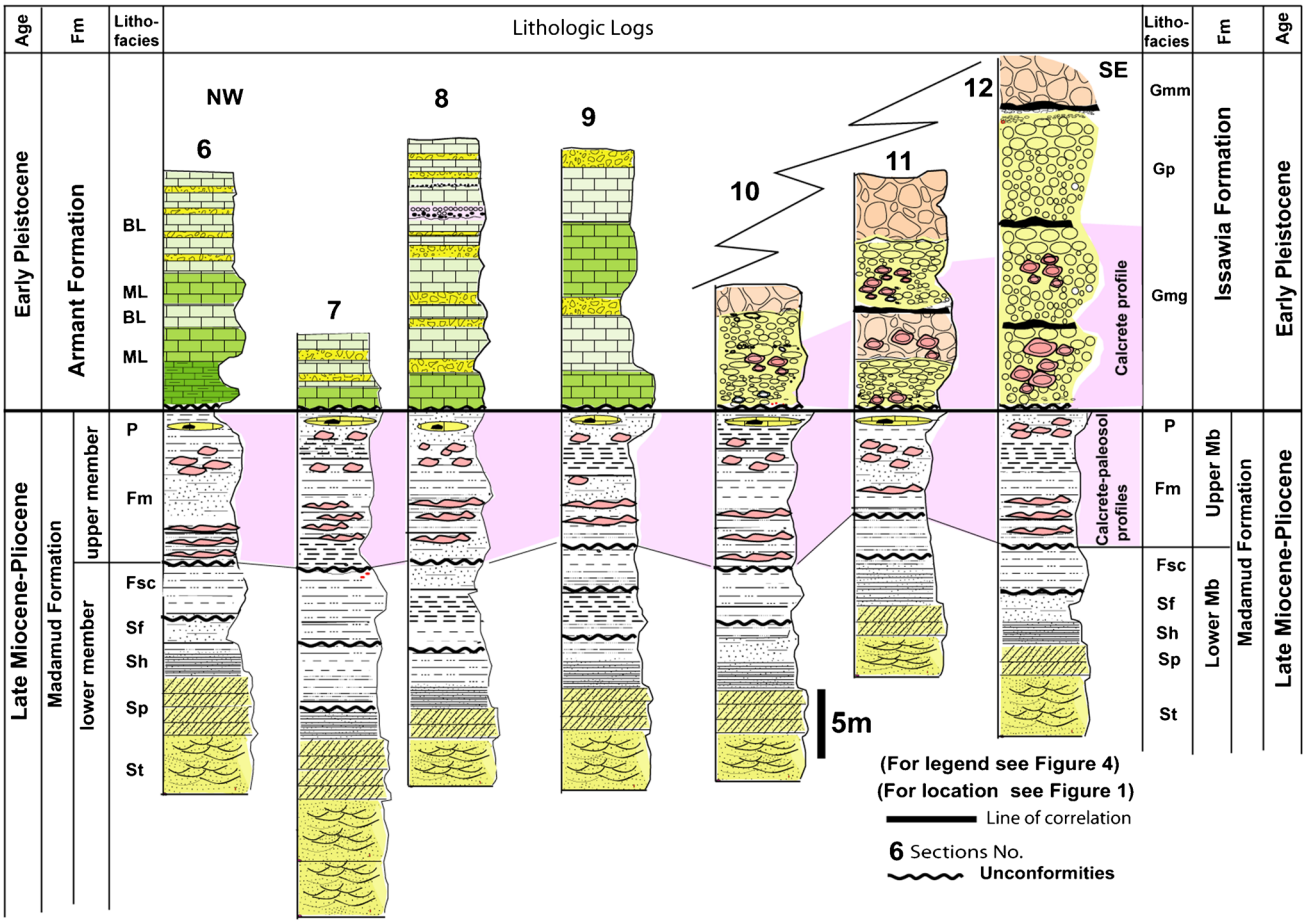

Fig. 6 NW–SE stratigraphic log correlation showing the along-eastern margin lithofacies changes of the fluvial lithofacies of the Madamud Formation and mixed fluvio-lacustrine lithofacies (Issawia and Arman Formations). Note the change in lithofacies associations above the line of correlation. In the north, carbonate is dominant. Towards the south, carbonates are shifted into coarse siliciclastics. Note the two calcrete profiles: mixed nodular-massive calcrete at the base and dominant nodular type in its upper part. Datum is on top of the Madamud Formation

(Fig. 5h). Cracks and dissolution channels developed during dry periods (Esteban and Klappa, 1983), which were filled later with sparry calcite cement.

Lithofacies Gmg: matrix-supported conglomerates

Lithofacies *Gmg* is the most frequent lithofacies type. Its thickness is about 30 m, representing ~ 70% of the Issawia Formation. In places, it interfingers laterally with *Gmm*. The beds of lithofacies *Gmg* tend to thicken and coarsen upward (Fig. 5g). The local conglomerate clasts are predominately composed of Eocene limestones and cherts. They are subrounded to rounded, and some are subangular; all are embedded in a coarse calcite and fine-grained sand matrix. Occasionally, the breccias and conglomerates are coated and cemented by calcretes. The conglomerate beds contain calcic paleosol intervals that vary in thickness from 10 to 50 cm. Locally in the top part, large blocks that are up to 2 m in diameter can be observed. Paleocurrent patterns from some imbricated clasts indicate transverse transport towards the axis of the basin.

Interpretation

The lack of stratification and the immature sorting support the debris-dominated alluvial fan environment. The progradation of proximal fan lobe deposits may be indicated by the thickening of the bed and the upward trend for coarsening (Tanner and Lucas 2018). Large boulders and blocks up to 2 m in diameter indicate flash floods accompanied by debris flows. Conglomerate deposits have been observed at the mouths of major wadis, suggesting that the location of the alluvial fans was controlled by debouching wadis that were inherited from previous ENE cracks in the surrounding limestone bedrock (Philobbos et al. 2000; Issawi and Osman 2008; Lansbery 2011). The clast constituents of the alluvial

fans are predominantly limestone and chert, reflecting the erosion of these clasts from limestone rocks outcropping close to the basin. The pedogenic processes, including rain wash, are thought to have created the paleosol intervals. This indicates that the alluvial fan deposits were abandoned, as it provides evidence of the ephemeral clastic discharges typical of the fans.

Lithofacies Gp: planar cross-stratified conglomerate

This lithofacies is grey in colour and is separated from the underlying lithofacies *Gmg* by an unconformity with an irregular erosional surface. It is distinguished by low-angle planar cross-bedding. The thicknesses of the cross-bed sets and their cosets are 0.5 to 1 m and up to 5 m, respectively. The dip of the foreset ranges from 10 to 20°. The beds are clast-supported with a sandstone matrix. Clasts range in diameter from 2 to 15 cm, are rounded to subrounded, and occasionally have an imbricated fabric.

Interpretation

This lithofacies is interpreted to have developed as a result of the migration of linguoid or transverse bars within a braided system or inside a gravel-bed meander stream (Miall 1977, 1978). It is believed that the unconformity of the surface with the underlying lithofacies *Gmg* indicates that much of this lithofacies emerged and was eroded before the overlying lithofacies *Gp* formed during the Early Pleistocene.

Lithofacies ML: massive limestone

This lithofacies consists of massive limestone beds. Most beds commonly grade vertically and laterally into the brecciated lithofacies that are described below (Figs. 5i and 6). These deposits consist of homogeneous without lamination limestone beds. Laterally, this lithofacies interfinger with the lithofacies associations of the Issawia Formation. Petrographically, the lithofacies *ML* are micrites with textures ranging from mudstone to wackestone, containing charophytes, gastropods, and ostracods (Fig. 7a–c). Gastropods are found as sparry calcite-filled moulds or preserved shells. In these limestones, polygonal desiccation fissures, sometimes filled with sparry calcite and usually well-defined throughout the whole bed, are encountered.

Interpretation

Lithofacies *ML* is dominated by lime mudstone and wackestone, indicating more open lacustrine deposition during highstands (Alonso-Zarza and Wright 2010), and suggests that deposition took place in conditions with relatively deep, low-energy lake water and an increased sedimentation rate (Abels et al. 2009; Adhikari and Wagreich 2013). These limestones include carophyta and small gastropods, which are indicative of a fresh to brackish lake environment (Sim et al. 2006). The existence of *ML* in the lower parts of the *BL* beds shows that the *ML* is a depositional residue and that the *BL* lithofacies, which is commonly overlying and laterally equivalent, was formed by modifying the tops of lithofacies *ML*. Similar massive limestone lithofacies that change laterally and vertically to brecciated have also been described in the palustrine limestone of south Spain (Miguel Nieto-Albert et al. 2022). It is suggested that the massive facies was deposited towards the centres of such lakes but was exposed episodically during lake regression. They were subjected to extensive pedogenesis during times of lowstand when desiccation fracturing and penetration of roots created brecciation.

Lithofacies BL: brecciated limestone

This lithofacies is well formed in the upper portion of the Armant Formation and increases closer to the western basin margin. In the outcrops, this lithofacies is thin-bedded either in individual beds (0.3 m thick), displaying multi-story ledges extending for hundreds of metres, which grade laterally to massive limestone. Most beds have a variety of fabrics, but not all of them are present in every bed. The most frequent feature of lithofacies *BL* is a brecciated fabric that covers the entire or a portion of the bed (Fig. 5k). The *BL* lithofacies are composed of subangular to angular clasts that were formed in situ throughout all of the beds. They range in size from 2 to 5 cm. The brecciated limestones include grains of quartz, bioclasts, and in some cases, chert fragments. All together, they are cemented by a microsparite. This lithofacies can be recognized by a variety of pedogenic features reported by some workers (e.g., Freytet and Plaziat 1982; Huerta and Armenteros 2005; Alonso-Zarza and Wright 2010; Tanner and Lucas 2012) and is composed of three fabrics: rhizolitic, intraclastic (Fig. 7d, e), and clotted-peloidal. Numerous root traces can be found, particularly towards the tops of the beds where they penetrate 15 cm, branching and tapering downward (Fig. 7f). In thin sections, the root traces are recognizable as elongate and irregular cavities filled with fine to coarse calcite. Vadose sparry calcite may occasionally fill channels, vugs, fenestrae, and pseudomicrokarst cavities, in addition to circumgranular cracks and fissures (Fig. 7g). Grainstone and packstone textures of clotted-peloidal fabric are embedded in sparitic and microsparitic calcite cement (Fig. 7h).

Interpretation

Lithofacies *BL* is typically thicker upwards in places near the western portion of the lake. This suggests that many

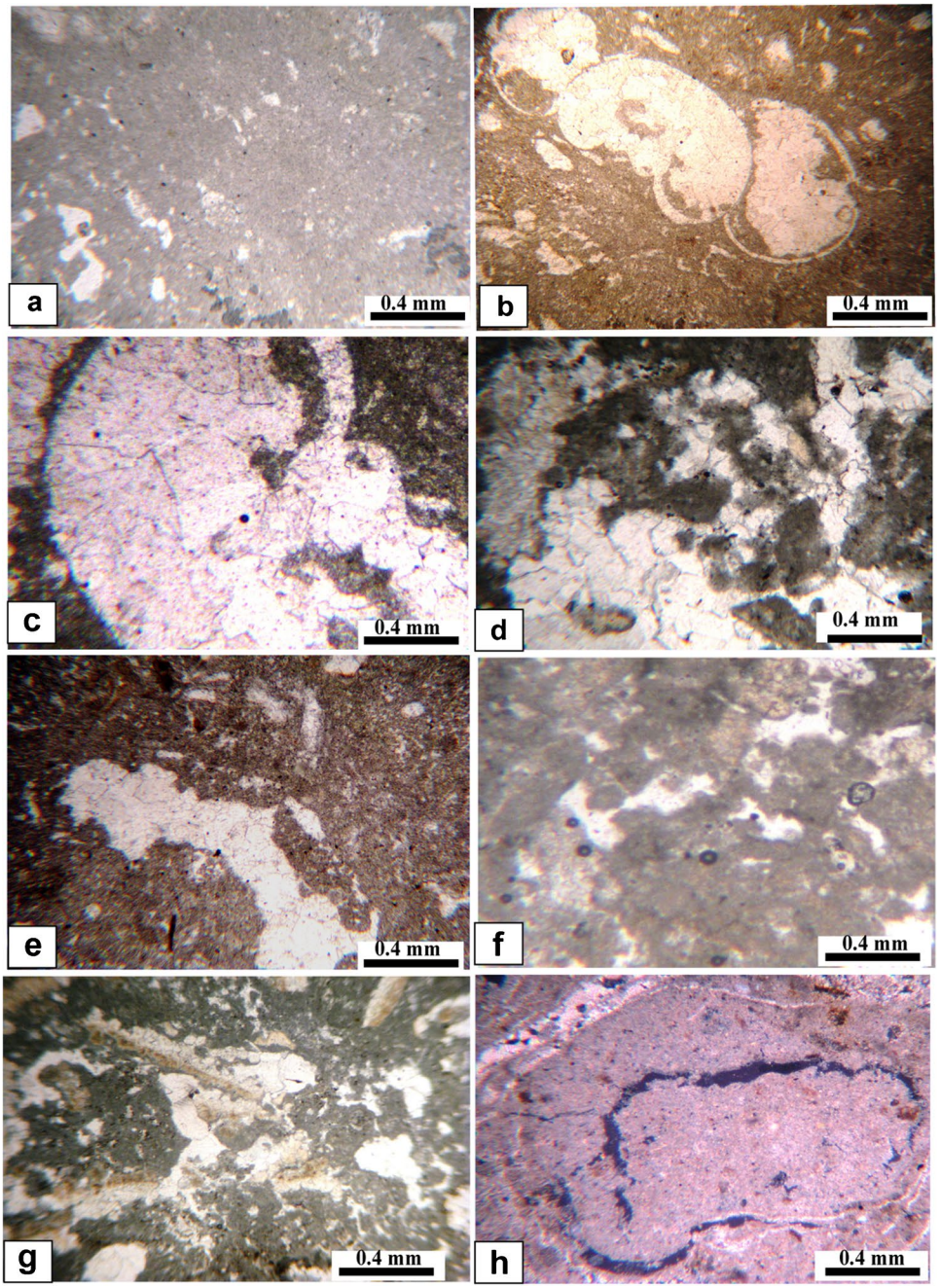

Fig. 7 Photographs showing lacustrine-palustrine limestone microfacies. **a** Lacustrine mudstone and wackestone with preserved charophytes. **b** Lacustrine limestone with abundant gastropods and charophytes. **c** Bioclast shells are replaced by vadose silt and blocky calcite. **d** Blocky calcite occurs as rectangular to square calcite crystals in shape with an irregular and planar outline. **e** Desiccated mudstone, in which the cracks are filled with sparry calcite. **f** Granular with intraclast limestones showing irregular desiccation cracks and clotted and peloidal grainstone fabric. Note that the cracks are not filled. **g** Nodular limestones, including irregular cracking networks. **h** Lacustrine wackestone showing planar and circumgranular cracks filled by vadose silt

sedimentation-exposure events had an impact on the entire lacustrine system and/or that the lacustrine system was created as a result of substantial subaerial exposure and modification (Alonso-Zarza et al. 2011). Clasts of lithofacies *BL* exhibit angular to subangular shapes, which lack any signs of rounding, indicating that the grains are formed in situ. Later, the fragments are affected by vadose and groundwater cementation (Alonso-Zarza et al. 1992; Alonso-Zarza and Arenas 2004).

The *BL* lithofacies exhibits a variety of pedogenic modifications, including rhizoliths, circumgranular cracks, mottling, and clotted-peloidal intraclastic fabrics. These features suggest that the lake basin had shallower, low-energy, and low-gradient margins and that it was subaerially exposed throughout the lowstands of the lake level (Platt and Wright 1992; Huerta and Armenteros 2005; Tanner 2000; Tanner and Lucas 2018). Comparable Miocene palustrine systems with fluctuating water levels have been documented for the Mediterranean (i.e., Arenas and Pardo 1999; Turkey; Alçiçek and Alçiçek 2014). The formation of vertical, downward-tapering fissures and clotted-peloidal intraclastic limestones supports long-term subaerial exposure and is

assumed to have resulted from repeated desiccations during episodes of falling water tables and shrinking water bodies when it was common for plant roots to penetrate the sediment (Plaziat and Freytet 1982; Huerta and Armenteros 2005; Alonso-Zarza and Wright 2010; Tanner and Lucas 2012). The occurrence of circumgranular cracks that have been filled with silt and sprite is thought to be attributed to cyclic drying and wetting (Alonso-Zarza and Wright 2010). Similar examples of carbonates with comparable fabrics that can be interpreted as lacustrine/palustrine deposits in the Middle Miocene intermediate unit at the Madrid basin (Alonso-Zarza et al. 1992), the Owl Rock Formation of the Chinle Group (Tanner 2000) and the Mid-Eocene unit in the Gebel El-Goza El-Hamra, NE Desert of Egypt (Wanas et al. 2015).

Calcretes

The calcrete levels typically develop in the lithofacies *Fm*, *Gmm*, and *Gp*, and they can range in thickness from 0.5 to 10 m. According to the calcrete classification of Netterberg (1980), Goudie (1983), and Wright and Tucker (1991), three main calcrete types were identified in the fluvial and fluvio-lacustrine succession based on the observed data and features (described below).

Mixed nodular-massive calcretes

The mixed nodular and massive calcretes are formed on the tops of the lithofacies *Fm* and alternate cyclically within them (Fig. 8a, b). The nodular calcretes are made up of nodules of diverse sizes and shapes that range in colour from white to light grey. They range in shape from subspherical to irregularly merging nodules that make up the concretionary calcretes. They are elongated and parallel to the strata of the sediment body (Fig. 8c, d). This type of calcrete has a lot of cracks, which are usually embedded with a mosaic of sparry calcite. Under a microscope, the matrix of the parent sediments can be seen to contain micrite nodules that make up the nodular calcrete. Quartz grains are floating in a micritic calcite groundmass to produce micritic nodules (Fig. 8e). Some of the quartz grains show etched features that are surrounded by a sparitic rim, forming a structure that resembles a corona (Fig. 8f, g). According to Wright and Tucker (1991), all of these characteristics point to an alpha microfabric. The nodular calcrete grades vertically into massive calcrete, and it has a colour variety that ranges from yellowish white to grey (Fig. 8h). The massive calcrete consists of flattened and stratified calcrete that forms a 0.5-m-thick layer above the nodular calcrete layers, and it is highly indurated. It also occurs as pillars filling mud cracks with slickensides and other shrinkage features (Fig. 8i). When examined under a microscope, it is a mosaic of microsparite calcite which ranges between 5 and 12 m in size. No biogenic features, including alveolar septal structure, calcified roots, or microcodium, are observed.

Interpretation

The mixed nodular and massive calcrete profiles indicate that they have been formed during periods of fluvial sedimentation and calcrete accumulation. Their integration into sedimentary successions provides support for sedimentary hiatuses. (Candy et al. 2003). Similar cyclic calcrete profiles are present in both the Miocene in the Duero basin (Armenteros and Huerta 2006) and the Hagoul clays (Khalaf and Gaber 2008). According to the interpretation of these authors, the transition from nodular to massive calcrete indicates the increase in carbonate concentrations relative to siliciclastic components. The gradual change indicates the floodplains' slow rate of sedimentation (Alonso-Zarza et al. 1992; Sanz et al. 1995). This could imply a gradual increase in the water table near the surface during episodic recharge of groundwater linked to low terrigenous sedimentation (Alonso-Zarza and Silva 2002; Candy et al. 2003; Alonso-Zarza 2003; Huerta and Armenteros 2005; Alonso-Zarza and Tanner 2006; Alonso-Zarza et al. 2011; Al Shuaibi and Khalaf 2011; Wanas and Sallam 2014). The lack of biogenic features, the prevalence of etched detrital quartz, a mosaic of microsparite calcite cements (5–12 μm in size), the sharp boundaries, and the lack of pedogenic textures suggest their groundwater origin and deposited in the phreatic zone (Mack et al. 2000; Jutras 2017; Alonso-Zarza and Wright 2010). Additionally, their groundwater origin is confirmed by the presence of pillar calcrete with its sparry calcite composition (Alonso-Zarza and Wright 2010; Jutras 2017).

Nodular calcretes

Nodular calcretes are the dominant calcrete type in the topmost part of the lithofacies *Fm*. The nodular profile is composed of vertically elongated clusters (20 cm in length and 6 cm in diameter, Fig. 8k) at the upper and isolated, dispersed, nearly spherical to irregular globular nodules (5 to 15 cm in diameter) at the bottom. As the carbonate concentration rises from the bottom to the top, the thickness of this profile changes from 2 to 8 m. Desiccation fissures, mottling, and diffuse margins are visible on the nodules (Fig. 9a).

Interpretation

Based on the disorganized pattern of calcrete nodules in the red siltstones and the presence of oxidation, the nodular calcrete is formed in the meteoric vadose zone (Huerta and Armenteros 2005). According to Khadkikar et al. (2000), these nodules may have been inorganically taken by meteoric

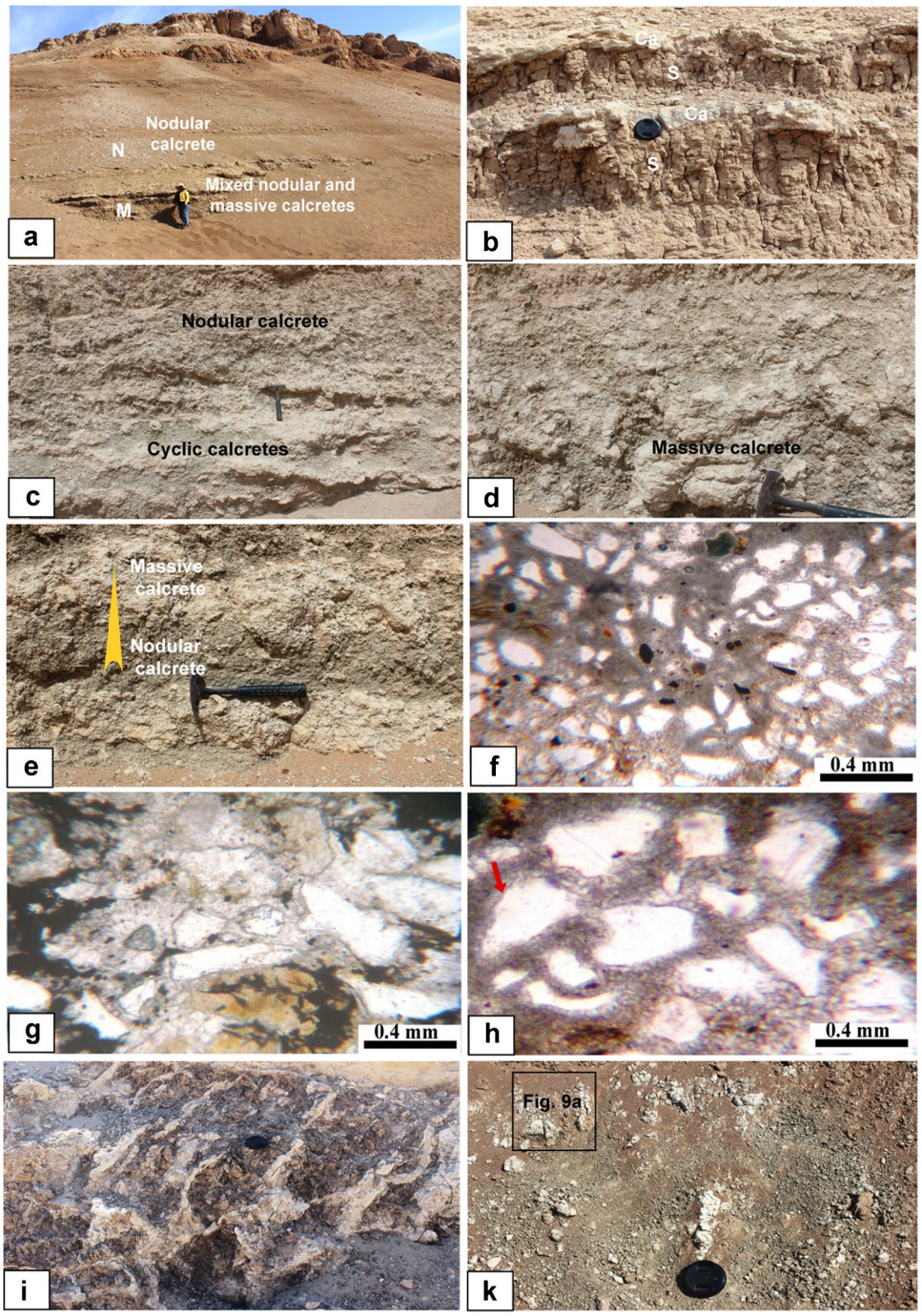

Fig. 8 **a** The nodular-massive calcrete is overlain by nodular calcrete, with a sharp boundary between them. The lower half is composed of mixed nodular-massive calcrete, while the upper half is made up of nodular calcrete. **b** A close-up view of alternated massive calcrete (M) and fine siliciclastics. Note that the massive calcrete displays sharp upper and lower boundaries (S). **c** Cyclic calcrete at the base followed upwards into nodular calcretes, **d** Subspherical to irregular coalesced calcrete nodules form the concretionary calcretes, which are elongated and parallel to the strata of the sediment body. **e** A photomicrograph of a massive calcrete reveals etched quartz grains coated by spar calcite cements and embedded in a micrite matrix. **f** A photomicrograph of massive calcrete in a calcisol showing Alpha microfabrics that mainly consist of microsparitic to sparitic calcite groundmass with floating quartz grains. **g** Enlargement part of **e** showing sparitic calcite-fringing quartz grain with a corona-like structure (arrow). **h** Nodular calcrete overlain by massive calcrete. Note the gradual transition from nodular to the massive calcrete (arrow). **i** Reddish brown mudstone with slickensides filled with massive calcrete (Pillar calcrete). **k** Nodular calcrete in reddish brown facies showing diffuse margins and exhibits a downward elongation

fluids because of their diffuse margin. They are caused by precipitating, displacement, and/or replacement processes that accumulate calcium carbonates in sediments and/or horizons of soil (Goudie 1983; Wright and Tucker 1991).

Coating and cementing calcretes

This type of calcrete profile dominates the lithofacies *Gmm* and *Gmg* of the Issawia Formation. Two calcrete fabrics displaying successional relationships are recognized: laminar-coated grains and calcrete cements (Fig. 9b). (a) The laminar-coated grains consist of gravel-sized clasts coated with hematite-stained, micrite bands. Internally, the bands occur as packages of rhythmic, individual laminae (0.2 to 0.3 mm in thickness, Fig. 9c) that are defined by their colour and laminae thickness. Tubiform laminae rich in alveolar septal structures are common. The package is laterally discontinuous and characterized by a downward elongation. (b) The calcrete-cemented fabric is infilling the interstitial spaces between coated breccias and conglomerate

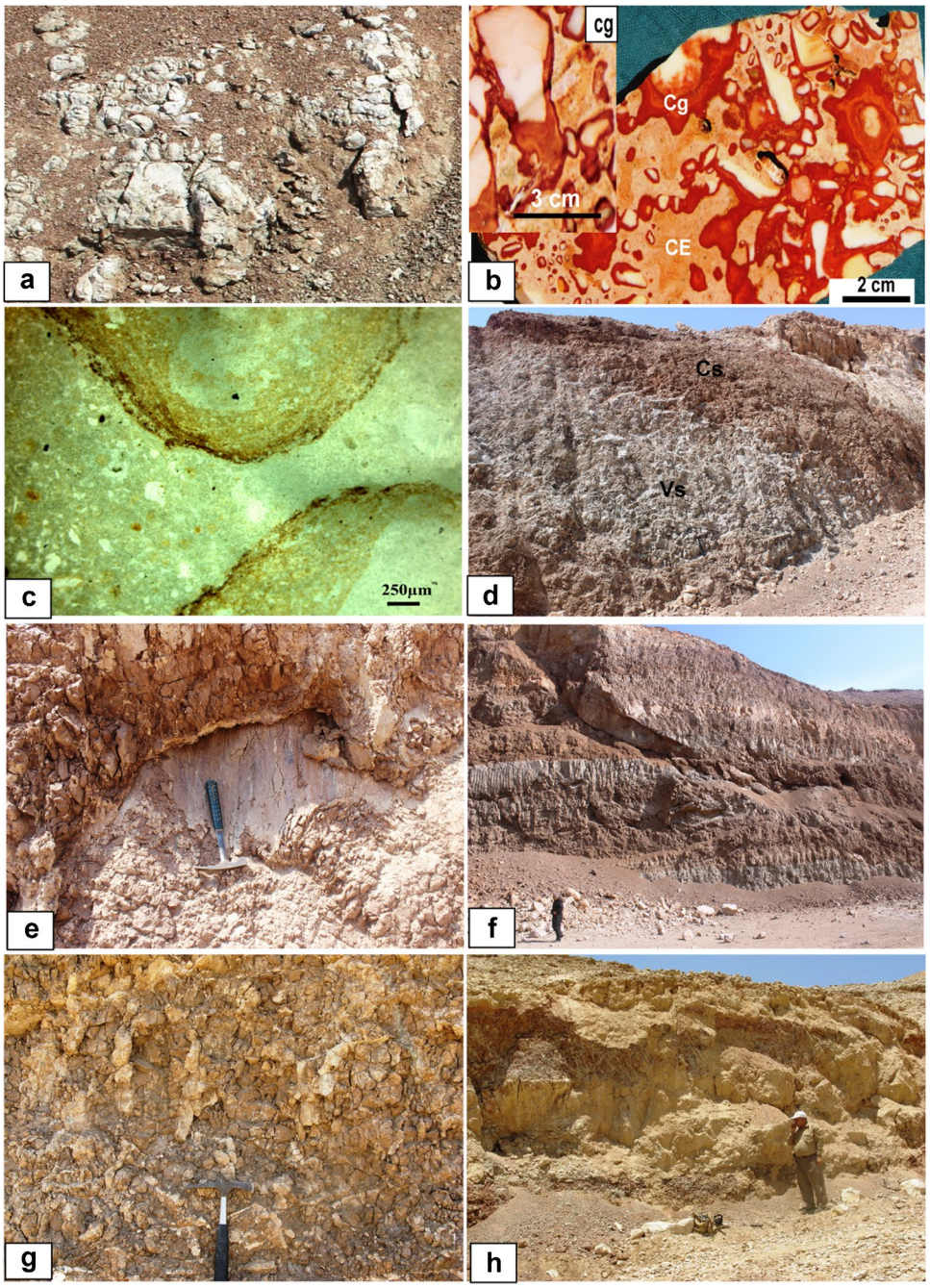

Fig. 9 **a** A square enlargement of Photo 8f, demonstrating nodular calcrete desiccation. **b** Polished slab showing laminar-coated grains are made up of gravel-sized clasts coated with hematite-stained micrite bands. In the upper left, enlargement of clasts encrusted by a downward elongation of laminar calcrete (cg). **c** A photomicrograph of laminar calcrete-coated grains. Note that the laminae are composed of dense micrite, with alveolar septal structures. The coated clasts are cemented by microspar and sparite, including some detrital quartz grains. **d** Field view showing the calcic paleosol (Cs) unconformably overlying the vertic paleosol (Vs). Note the vertisols showing prominent vertic fractures. **e** A close view showing slickenside planes, with polished surfaces and striations in the vertic paleosols. **f** Large desiccation cracks and pseudo-anticlines in the calcic paleosol. **g** Calcic paleosol displays evidence of pedoturbation in the form of rhizoliths or calcified roots. **h** Calcic paleosol includes massive calcrete

clasts. Microscopically, the cementing calcrete is made up of equal parts of microsparite and sparite mosaics (Fig. 9b).

Interpretation

The prevalence of micritic coating, pisoids, and limestone nodules in the laminar-coated grain fabric, as well as their proximity to the surface of the beds, indicates that pedogenic processes were primarily responsible for calcrete production. The presence of biogenic microstructures (e.g., root tubes, alveolar septal structures, and calcified roots) supports the pedogenic origin (Alonso-Zarza 2003; Alonso-Zarza and Arenas 2004; Huerta and Armenteros 2005). The downward elongation of the lamination implies that in situ processes were responsible for their growth. The occurrence of equal mixtures of crystalline sparite and microsparite mosaic types of cement filling interstitial voids implies that elevated groundwater levels could have been a significant factor in the production of calcrete. The successional relationship between the laminar-coated grains and sparry calcite cement proved that the latter had not formed by the recrystallization of previously present laminar micrite. Therefore, according

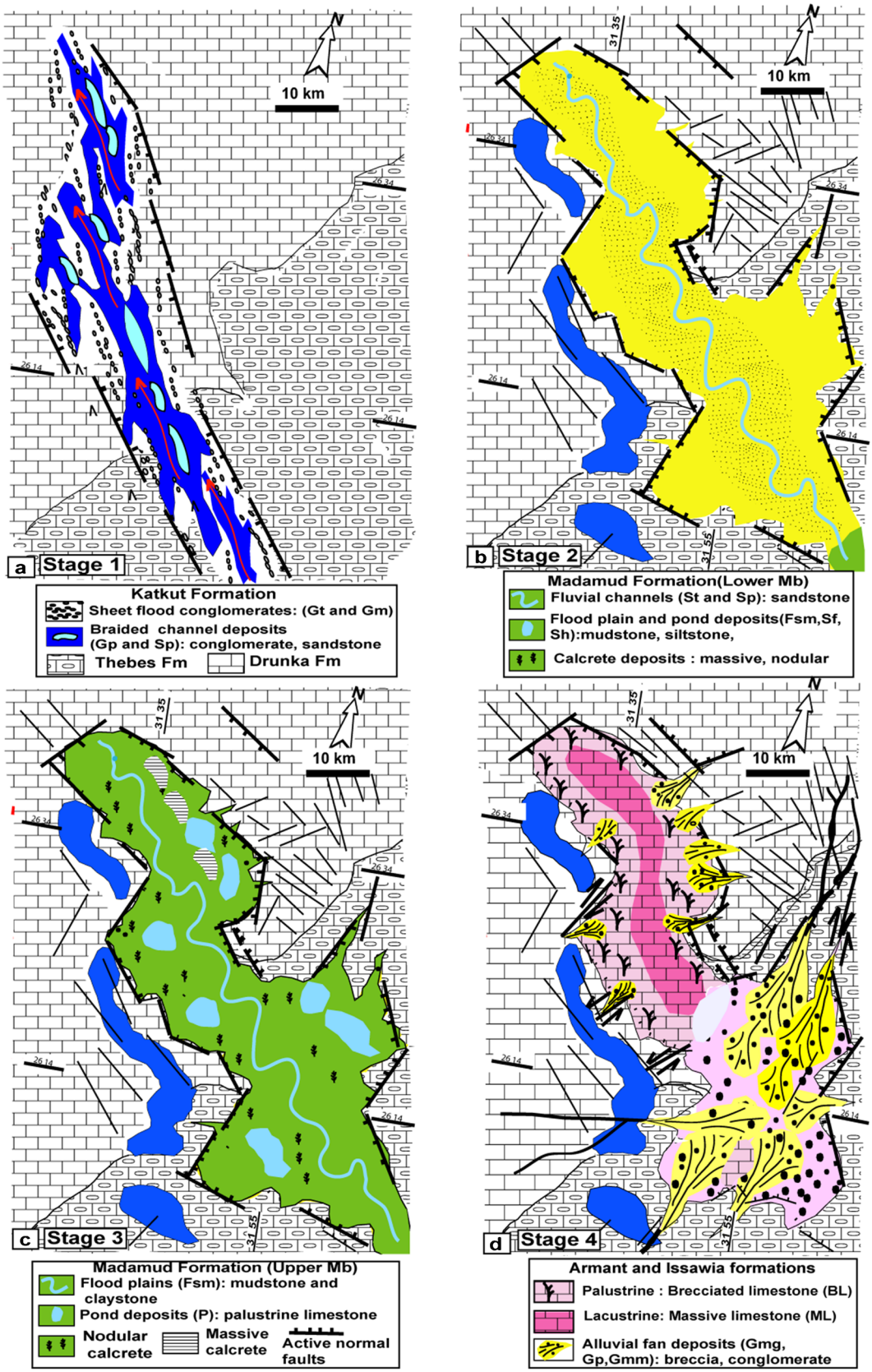
a Stage 1
10 km
N
Katkut Formation
Sheet flood conglomerates: (Gt and Gm)
Braided channel deposits (Gp and Sp): conglomerate, sandstone
Thebes Fm
Drunka Fm
b Stage 2
10 km
N
Madamud Formation(Lower Mb)
Fluvial channels (St and Sp): sandstone
Flood plain and pond deposits(Fsm,Sf, Sh):mudstone, siltstone,
Calcrete deposits : massive, nodular
c Stage 3
10 km
N
Madamud Formation (Upper Mb)
Flood plains (Fsm): mudstone and claystone
Pond deposits (P): palustrine limestone
Nodular calcrete
Massive calcrete
Active normal faults
d Stage 4
10 km
N
Armant and Issawia formations
Palustrine : Brecciated limestone (BL)
Lacustrine: Massive limestone (ML)
Alluvial fan deposits (Gmg, Gp,Gmm): breccia, conglomerate

◂**Fig. 10** Interpreted paleogeographic reconstructions of the four evolutionary stages of the Sohag basin. **a** In stage 1, in the Late Oligocene, the basin was formed by a regional extension, leading to the deposition of the sheet floods and braided channel deposits of the Katkut Formation. **b** In stage 2, in the Late Miocene, the basin continued to subside accompanied by a humid climate leading to the deposition of the channels and floodplain deposits of the lower member of the Madamud Formation. **c** By Pliocene, in stage 3, the basin continued to sedimentation accompanied by an arid climate leading to the deposition of floodplain, calcrete, and palustrine deposits of the upper member of the Madamud Formation. **d** In stage 4, by the Early Pleistocene, the basin was dissected by the ENE- and NNE-trending fault strands, leading to the deposition of the alluvial fans of the Issawia Formation, which developed along basin margins and transversed into the axis of the basin, interfingering with longitudinal lacustrine carbonates

to the calcrete stratigraphy, coated grain calcrete seems to have evolved first, and interstitial spaces were subsequently filled with microsparite and sparite mosaic cements. Similar relationships between laminar-coated grains and sparry calcite cement have been described in the Teruel Graben, northeast Spain (Alonso-Zarza and Arenas 2004).

Paleosols

The presence of palaeosols, which have a combined thickness of around 10 m, is a distinctive characteristic of the overbank deposits (upper member of the Madamud Formation). They consist of continuous tabular beds that range in colour from greyish-white to brown. The interior structure of these palaeosols ranges from massive to blocky. The most noticeable pedofeature is the presence of calcium carbonate, which may take the form of small nodules or massive calcretes. According to Mack et al.'s 1993 classification, paleosols can be divided into two main types: vertic and calcic.

Vertisols

Vertisols are abundant in the lowest portion of the upper member of the Madamud Formation. Although their lateral extent extends hundreds of metres, channel-fill deposits of lithofacies *Sp*. frequently cut them. Its predominant lithology is sandy mudstone whose thickness ranges from 0.2 to 0.5 m, and its colouration ranges from grey to greyish white (Fig. 9d). It has scattered small carbonate modules with spherical to subspherical forms, up to 1 cm in diameter. The nodular carbonates can be found as veins or scattered nodules (2–4 mm in diameter) to massive coalescent nodules (up to 5 cm in diameter). Among the recognizable diagnostic features are slickenside planes, which are laterally continuous with polished surfaces and striations (Fig. 9e). Mineralogically, the vertisol fractions exhibit high proportions of kaolinite relative to other clay fractions (Mahran and Hassan 2023).

Interpretation

The most obvious indicators of expandable clays shrinking and swelling can be found in these vertisols (Kraus and Aslan 1999). Clays, which formed as a result of repeated wet-dry episodes, shrank and swelled as evidenced by the presence of bowel-shaped slickensides (Retallack 2001; Abdelfattah 2021). The high content of kaolinite implies generally well-drained soils (Sheldon and Tabor 2009), while the presence of carbonate nodules, veins, and streaks is related to low water tables during dry seasons (Retallack 2001; Kraus and Hasiotis 2006).

Calcisols

Calcisols terminate the upper member of the Madamud Formation and are interbedded with breccias and conglomerates of the Issawia Formation. The calcisols of the Madamud Formation consist of tabular beds with a lateral extension of several kilometres. The upper contact has an erosional surface with dissolution features, whereas the lower contact is erosive. Pseudo-anticlines and large desiccation cracks are also observed (Fig. 9f). The most noticeable pedofeature is the presence of calcium carbonate, which can take the form of small nodules or massive calcretes (Fig. 9g, h). Three distinct types of alpha microfabrics were identified: floating detrital grains, etched quartz grains, and calcitic crystalline grains enriched with calcite groundmass.

The calcisols of the Issawia Formation are also reddish brown in colour and are up to 50 cm in thickness and repeated in three horizons. This paleosol is found on the tops of the gravels. The upper part of the paleosol is truncated and buried under the overlying conglomerate cycles. The most common pedofacies are Fe/Mn nodules. Other pedogenic carbonate nodules are also present.

Interpretation

The development of calcisols is related to strong evaporation and average precipitation below 1000 mm (Beilinson et al. 2013). This hypothesis is reinforced by the occurrence of dolomite minerals in the upper strata (Mahran and Hassan 2023). The overall increase in smectite content relative to other clay minerals (Mahran and Hassan 2023) is thought to reflect a low-lying and poor-draining environment (Thiry 2000). According to Lindbo et al. (2010), the formation of Fe/Mn is attributed to the accumulation of water in poor permeability mudstones in a water-saturated environment.

Discussion

Depositional model

The distribution of fluvial- and fluvio-lacustrine facies associations during the Late Oligocene–Early Pleistocene allowed for the development of a depositional model in the following 4 stages:

In the first stage (Late Oligocene), the basin evolved as a full graben (Fig. 10a) with significant NW–SE extensional fault segments on the east and west of it (Mahran and Hassan 2023). The fault-bounded western margin was more active relative to the eastern one because the basin's depocenter was near the western boundary, where fluvial lithofacies *Gt*, *Sp*, *Gp*, and *Gm* of the Katkut Formation formed. These deposits were developed by pre-Eonile paleorivers that drain northwesterly (Issawi and McCauley 1993; El-Baz et al. 2000; Robinson et al. 2000; Ghoneim et al. 2007; Lansbery 2011; Abdelkareem et al. 2012).

In the second stage (Late Miocene), the basin continued as a fully NW–SE graben that was bounded by significant extensional fault segments to the east and west (Fig. 10b), some of which were linked by strike-slip faults (Mahran and Hassan 2023). As a result, the basin became deeper, and fluvial channels (lithofacies *St* and *Sp*) formed longitudinally (N-S) along the basin axis. Subsequently, sediments from the flood plain were vertically aggraded and accumulated in the centre and in near-shore areas (*Sh*, *Sf*, *and Fsc*). By the end of this stage, a few small lakes and ponds had formed on the flood plains; these lakes and ponds are more abundant in the vicinity of the active faults and associated hanging walls.

In the third stage (Pliocene), the basin experienced low terrigenous sedimentation events interrupted by periods of stagnation. These circumstances led to the accumulation of red mudstones (*Fm*), which alternated with cyclic nodular and massive calcretes (Fig. 10c). These cycles merged laterally, and in areas of more subsidence, mature, thicker, and massive calcretes completely replaced the red mudstones (Fig. 11).

In the fourth stage (Early Pleistocene), another phase of uplifting pulses started, and the physiography of the basin tilted largely eastward as it changed from a complete graben to a half-graben basin. As a result, multiple alluvial fans made up of breccias and conglomerates from the Issawia Formation (*Gmm*, *Gmg*, and *Gp*) accumulated. Some of these fans developed along the basin's margins and are limited in size, while others were transported from fault-bounded basin margins and transversely along the basin axis. At this stage, shallow lacustrine carbonate deposits (*ML*, *BL*) of the Armant Formation were accumulated towards the basin centre and laterally interfingered with the Issawia Formation (Fig. 10d).

Tectonics control on sedimentation pattern

Tectonics indicates that the main structural regime of the middle section of the Nile, including the Sohag basin, was created by the rifting of the Red Sea and Gulf of Suez during the Late Oligocene and Miocene (Youssef 2003; Sakran et al. 2019; Abdelkhalek and Jonas 2019; Abdelkhalek et al. 2020). This tectonic movement produced significant drops in the eustatic sea level by the end of the Eocene (Haq et al. 1987), as shown by the existence of a regional end-Eocene unconformity that separates Late Oligocene deposits from Eocene rocks (labeled "the end Eocene unconformity"). The long duration of this unconformity is demarcated by the absence of lower and middle Oligocene strata in the study area. Furthermore, the angular unconformities between the studied sequences (labeled "end Late Oligocene, end Late Miocene, and end Pliocene") that appear to be of regional extent across the studied area are linked to tectonic reactivation of the NW-striking faulting that defines the Sohag Basin. The local unconformities through the lithofacies *St*, *Sp*, and *Sf* (Fig. 12a) and evidence of synsedimentary soft-deformational structures (e.g., wedge geometry, faults, slumps, dykes, and breccias; Fig. 12b–g) support that they may be associated with tectonic influence on the accumulation of the studied deposits. Their occurrence in different stratigraphic levels was ascribed to basin subsidence and repetitive fault movements.

Additionally, this tectonic activity had an impact on the syn-rift Sohag basin's structure as well as the A/S ratio (i.e., accommodation space relative sediment supply) throughout the development of the Late Oligocene-Early Pleistocene sedimentary sequence. The lithofacies *Gt*, *Sp*, *Gp*, and *Gm* are linked to extensive fluvial activity, limited accommodation, and declining subsidence rates (Alonzo Zarza et al. 2011; Wanas et al. 2015; Scherer et al. 2015).

The channels and flood plain deposits (*St*, *Sp*, *Sh*, *Sf*, *Fsc*, and *Fm*) of the Madamud Formation most likely developed during periods of high accommodation rates and flooding. This is supported by the widespread onlapping and retrogradational stacked flood plain fluvial deposits (Fig. 12h, i). Floodplain sediments may build up due to tectonic subsidence and an increase in accommodation space compared to the sediment supply (Alonzo-Zarza et al. 2011; Scherer et al. 2015).

The overlying Issawia and Armant formations (Early Pleistocene) were also significantly influenced by tectonics (Guiraud et al. 2001). The lithofacies *Gmm* deposited against NW fault lines (fault scarps talus), whereas the lithofacies *Gmg* and *Gp* (alluvial fans) are affected by the transverse wadis, which inherited the NE-fault lines. Tectonics also played a major role in the distribution of the calcrete and lacustrine-palustrine deposits, as the lake basin's physiography displayed a typical east–west topographical gradient.

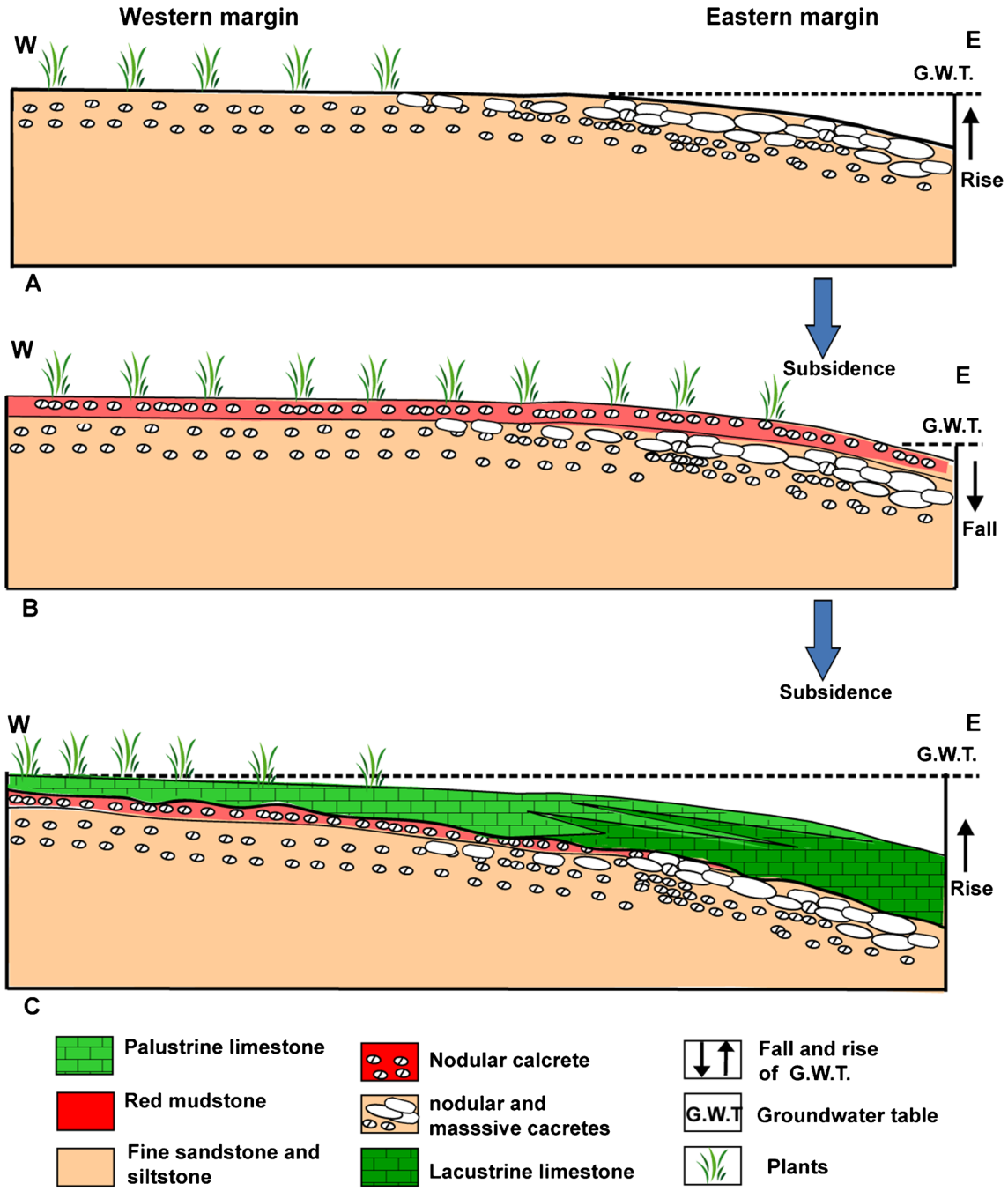

Fig. 11 A sedimentological model showing the control of hydrological conditions and subsidence on the lateral and vertical calcretes and palustrine-lacustrine deposition from the western to eastern margins of the basin. **a** Lateral and vertical transition from nodular to massive calcrete. **b** Formation of pedogenic nodular calcrete. **c** Lateral transition from palustrine, mixed palustrine–lacustrine to dominant lacustrine limestone

For example, the calcrete facies in the western margins occur as single, thin nodular-massive sequences and are strongly defined at the top of the alternated siliciclastics. Towards the east, they integrate into thick massive calcrete beds producing a fringe marking the lacustrine limestone from the distal fluvial facies (Fig. 11). Similar observations are observed from lacustrine-palustrine deposits. The palustrine lithofacies predominated the western margin of the basin due to its shallow setting and lower gradient. Where there is a high gradient on the eastern side, lacustrine and palustrine carbonate regressive cycles are more prevalent (i.e., A/S > 1). Alonso-Zarza et al. (2011) stated that the creation

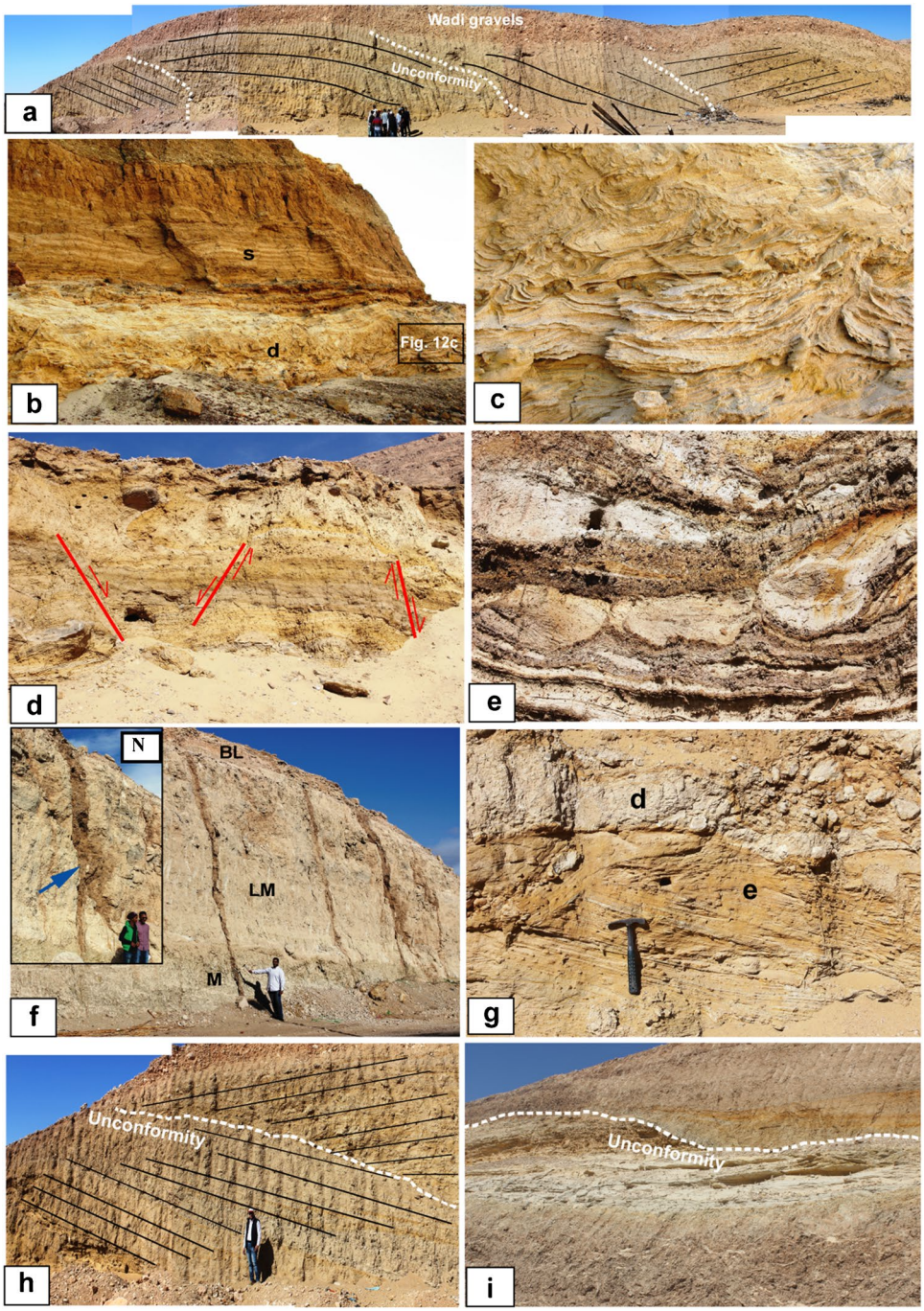

Fig. 12 Synsedimentary soft-deformational structures within the studied deposits. **a** Tilted thin-bedded sandstone and siltstone showing progressive thickenings towards the east (wedge-shaped pattern). **b** The deformed beds (d) were sealed by nondeformed mudstone and claystone (s). Note the effect of the deformation in the sandstone deposits with common slumped and folded beds. **c** Slumping in sandstone beds. Note the sandstone beds are dislocated and folded during flow and deposition. **d** Synsedimentary faults created grabens and horsts. Note this deformation is stratiform and coincides with the sandstone beds. The overlying beds are not affected by faulting. **e** Hydrobalstic (load cast) in interbedded sand and mud layers. Note that the internal bedding is deformed into sand lobes that are layered on top of one another and are pinched and stretched as a result of distensional movement. **f** Parallel fissure fillings cut through bedded fluvial mudstone (*M*) and lacustrine limestone (*LM*). Note enlargement isolated megafissure (*N*) infilling with clasts is derived both from the collapse of the overlying brecciated limestone (*BL*) and from the adjacent limestone and mudstones. **g** Boudinage structure is localized within alternating sand and mudstone beds, where the mud beds are dislocated into spaced fragments that locally float within the sand matrix. **h**, **i** End-Late Miocene angular unconformity occurs at the top of the lower Member of the Madamud Formation. Note that the upper member is onlapped into the underlying member

of stacked regressive cycles is hypothesized to be caused by strong pedogenic alteration during subsidence pulses and recurrent periods of subaerial exposure.

Paleoclimate changes

Paleoclimate and base-level changes have the greatest impact on alluvial and fluvio-lacustrine stratigraphic architecture changes in any basin (Holbrook et al. 2006; Turkmen et al. 2007; Pla-Pueyo et al. 2009; Bourquin et al. 2010; Huerta et al. 2011; Feng et al. 2013; Wanas et al. 2015; Scherer et al. 2015) where the paleoclimate directly conditioned the balance between sediment supply and accommodation (Beilinson et al. 2013). Tanner (2000, 2010) reported that sequences consisting of both lacustrine and palustrine carbonates are controlled mainly by climatically controlled fluctuations in base level, where the sediments of palustrine carbonates are subjected to intense pedogenesis under semi-arid conditions during the falling base level. Furthermore, the pedogenic characteristics of palustrine limestone, such as

desiccation fissures, brecciation, mottling, and nodularization, can provide evidence for the influence of water table changes and paleoclimate (Alonzo-Zarza and Wright 2010; Alonzo-Zarza et al. 2012).

In the study area, detailed sedimentological studies through the evolution of the architectural fluvial and fluvio-lacustrine facies and environmental changes, as well as the associated pedogenic characteristics, record paleoclimatic conditions changing throughout time (Fig. 13). The Katkut Formation is made up of various fluvial types, such as braided river and hyperconcentrated stream flow deposits, which, according to Picford et al. (2008) and Abdelkareem et al. (2012), indicate greater precipitation in the source regions (south and southeastern Egypt) during the Late Oligocene humid periods. This denotes a condition in which there is limited accommodation space. Additionally, this fluvial system displays characteristic fluvial incisions indicating periods of severe rainfall (Abdelkareem et al. 2012) as well as a large capacity for transportation (Nador et al. 2007). The prevalence of silicified limestone gravels, as well as widespread well-rounded cherts and quartz pebbles in lithofacies *Gt* and *Gp*, is said to have been produced by extreme chemical weathering in the source area (Selley 1982; Iwaniw 1984) and suggests deposition in an energetic fluvial environment in a humid tropical climate (Gürbüz et al. 2021). The presence of root moulds in the lithofacies *Sp* supports a subtropical to tropical climate with annual precipitation of 1200–1500 mm during the Oligocene–Miocene

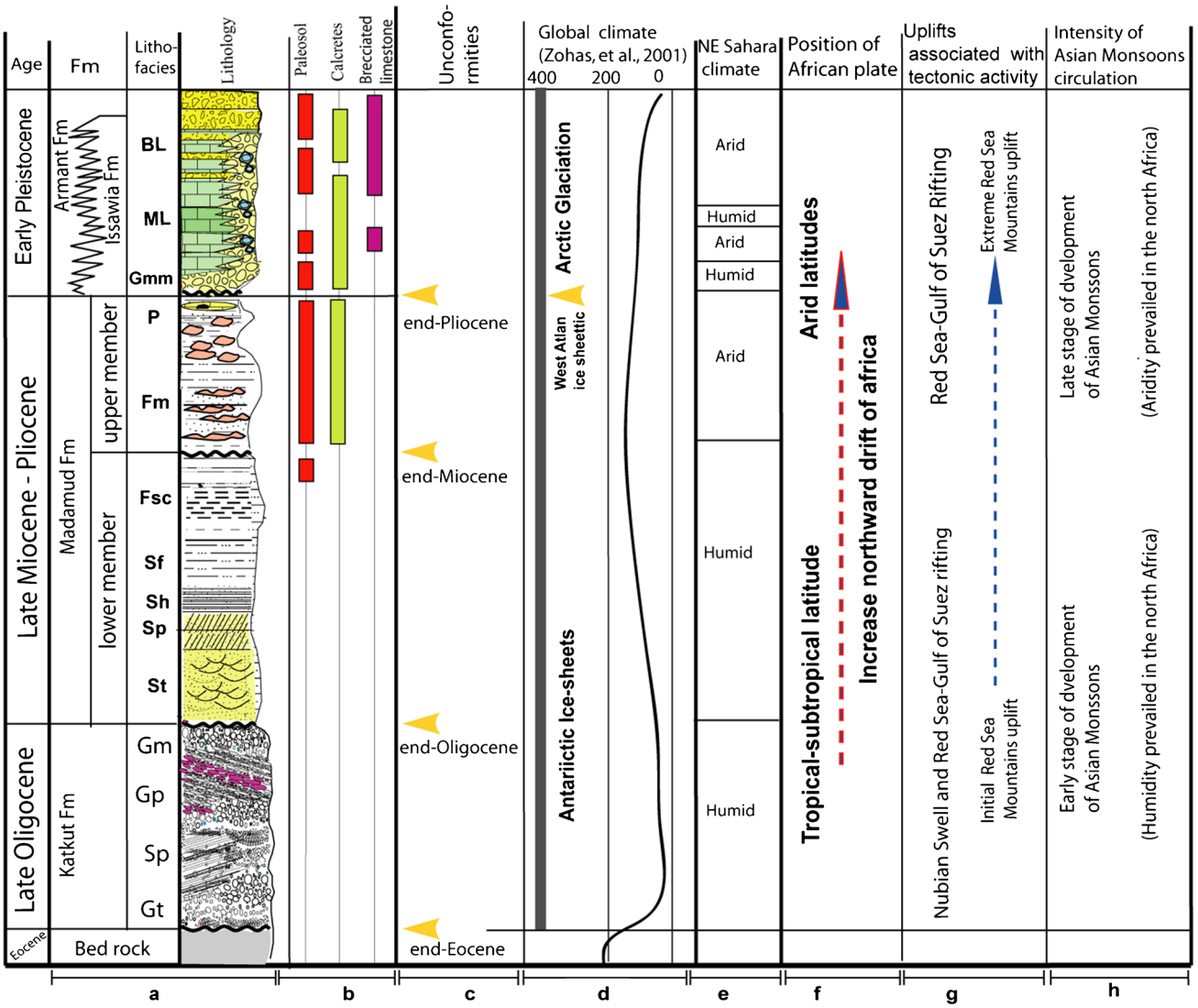

Fig. 13 Conceptual diagram summarizing the Late Oligocene–Early Pleistocene depositional history of the Sohag Basin, including **a** Stratigraphic succession, **b** vertical distribution and relative abundance of paleosols, calcretes, and brecciated limestone. **c** regional unconformities. **d** Global climatic events. **e** NE Sahara climate showing trends in climate towards more arid conditions. **f** Position of Africa plate. **g** Uplifts associated with tectonic events. **h** Source rocks. Trends in climate towards more arid conditions

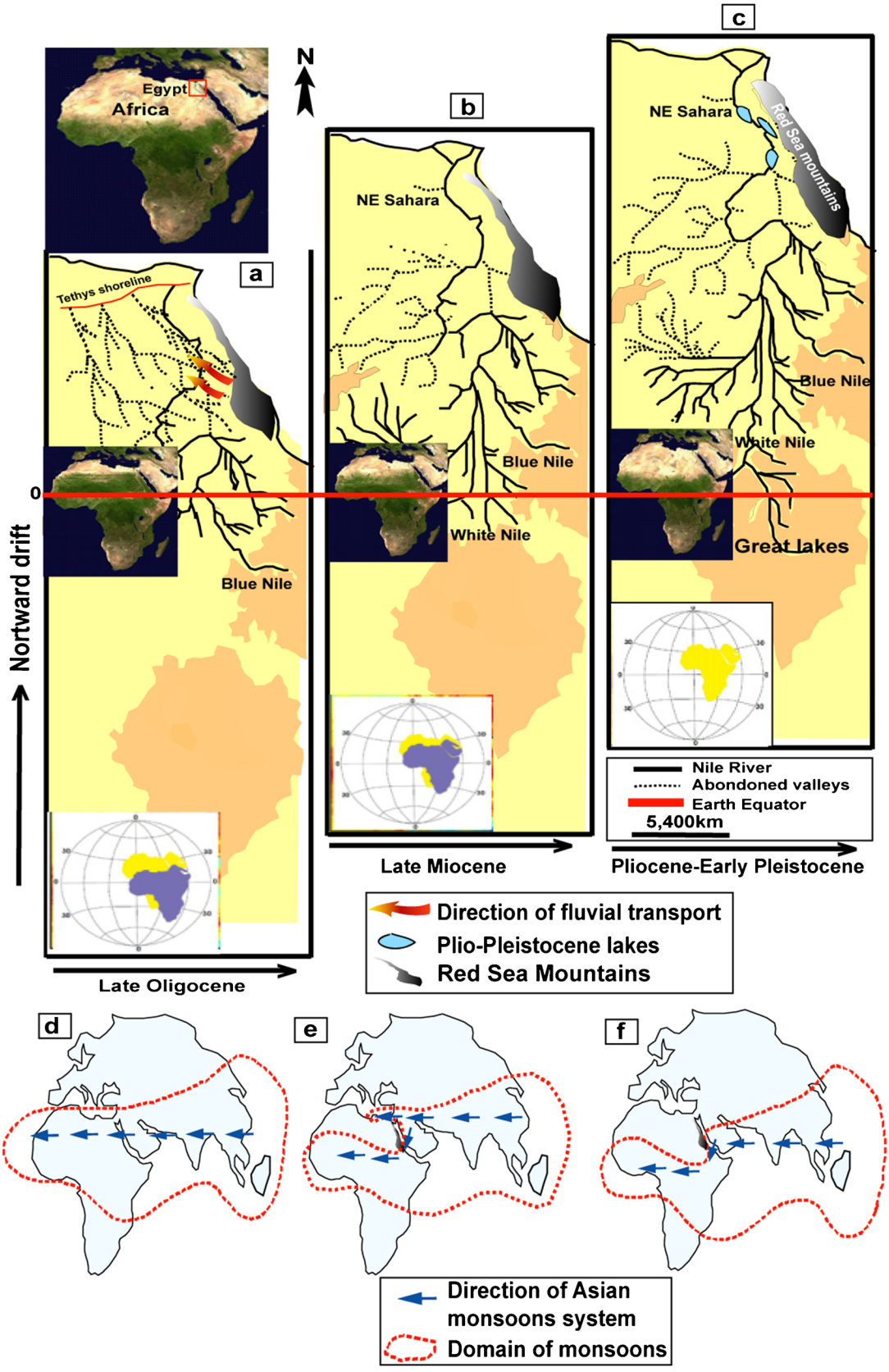
Egypt
Africa
N
a
b
c
Tethys shoreline
NE Sahara
Red Sea mountains
Blue Nile
White Nile
Great lakes
0
Norward drift
Late Oligocene
Late Miocene
Pliocene-Early Pleistocene
Nile River
Abondoned valleys
Earth Equator
5,400km
Direction of fluvial transport
Plio-Pleistocene lakes
Red Sea Mountains
d
e
f
Direction of Asian monsoons system
Domain of monsoons

◂**Fig. 14** Stages of the evolution of climate change in the Sahara region as a result of the northward drift of the African continent and movements of Asian monsoons. The solid red line indicates the Earth's Equator relative to the drifting continent. **a** The paleogeographic position of Africa during the Late Oligocene taken from literature (e.g. Smith et al. 1994; Swezey 2009; Abdelkareem et al. 2012). **b** The paleogeographic position of Africa during the Late Miocene, taken from literature (e.g. Smith et al. 1994; Swezey 2009; Abdelkareem et al. 2012). At this stage, deep incision and north-flowing rivers (Eonile Rivers) penetrated downwards to reach the Paleozoic and Mesozoic rocks. **c** Paleogeographic position of Africa during the Pliocene–Pleistocene taken from literature (e.g. Smith et al. 1994; Swezey 2009; Abdelkareem et al. 2012). **d** The circulation of Asian monsoons occurred during the Late Oligocene–Late Miocene. **e** The circulation of Asian monsoons occurred during the Early Pliocene. Note the uplifts of the Red Sea Mountains and the deflection of monsoons southward. **f** The southward movement of monsoon domains during Pliocene–Early Pleistocene time

(Nador et al. 2007; Picford et al. 2008; Issawi and Osman 2008). The humidity that predominated at that time is supported by the diversity of vegetation and the existence of clay and fossilized bones in karst caverns in the Western Desert's Farafra Oasis (Wanas and Sallam 2014), as well as by the abundance of vertebrate and reptile fauna, as well as tropical flora, in time-equivalent sediments located at north Fayum depression (Said 1990; Issawi and Osman 2008). In the study area, the humidity is documented by the predominance of fluvio-karstic landforms (e.g., cone karst, karren, giant flutes, fluvial channels, and paleodolines) in the surrounding limestone plateau (Grimes 2012; Mahran and Hassan 2019).

Humidity in the area significantly increased during the lower member of the Madamud Formation (*St*, *Sh*, *Sf*, and *Fsc*). The broad fluvial sand incision, which includes root moulds and subrounded to rounded quartz grains at the base, followed by the predominance of flood plain, grey-coloured mudstone deposits (Mahran and Hassan 2023), supported the prevailing humidity during that time. Their widespread occurrence exhibits aggradational stacking patterns throughout the basin due to the high accommodation during the base-level rise, sustained by persistent humid periods and/or tectonic subsidence (Tanner 2000; Armentores and Huerta 2006; Cabaleri et al. 2013; Tanner and Lucas 2018; Wanas et al. 2015). These lithofacies are composed primarily of kaolinitic clays (Mahran and Hassan 2023), which are not present in overlying lithofacies and are considered a strong indicator of a humid-subtropical to tropical setting and active soil material weathering (Chamley 1989; Hallan et al. 1991; Righi and Meunier 1995; Ruffell et al. 2002).

Climate was also a fundamental control on the development of calcretes and paleosols in the lithofacies *Fm* (upper member of Madamud Formation). For example, the massive calcrete-clastic cycles can be interpreted as fifth-order fluvial aggradation cycles (Atchley et al. 2004), where variations in base level brought on by climatic oscillations induce cycles in accommodation and sediment supply. The overlying nodular calcretes display meteoric vadose origin, suggesting well-drained floodplains in an arid climate (Mack et al. 1993; Kraus 1999; Alonso-Zarza 2003). Gürbüz et al. (2021) suggested palaeoclimatic fluctuations according to the colours of the fluvial sediments in the Beyşehir-Suğla basin, Turkey. Accordingly, the lower, grey-coloured lithofacies *Sf and Fsc* indicate humid conditions, whereas the upper, brown–red-coloured lithofacies *Fm* suggest arid conditions. In addition, lithofacies *Fm* display the development of vertic and calcic-type paleosols that document the arid conditions (Tanner and Lucas 2006).

The fluvio-lacustrine deposits (Issawia and Armant formations) with extensive pedogenic features are also linked primarily to climate and base-level fluctuations, similar to those described by Tanner (2000) in the Owl Rock Formation of the southwestern USA. However, tectonics played an important role. According to Platt and Wright (1992) and Alonso-Zarza (2003), massive limestone (*ML*) has colour mottling, root traces, and desiccation cracks, which indicate intermittent dry periods.

Furthermore, the occurrence of various palustrine facies (such as clotted-peloidal, pseudomicrokarst, brecciated to granular limestone, and desiccated limestone) as a result of shrinkage cracking and desiccations during the emergence periods indicates that the climate was extremely arid (Platt and Wright 1992; Tanner 2000; Alonso-Zarza and Wright 2010; Alçiçek and Jimenez-Moreno 2013; Wanas and Soliman 2014; Tanner and Lucas 2018). Additionally, such arid conditions associated with base level lowstand caused the interbedded and the lateral equivalent ephemeral fluvial deposits (*Gmg* and *Gp*) with scour bounding surfaces, analogous to the interpretation of the fluvial system in the Triassic San Pedro Arroyo Formation (Tanner and Lucas 2012). The aridity is supported by the presence of calcisols and carbonate-rich rock fragments. Furthermore, the overlapping of calcrete fabrics (vadose, and groundwater) indicates that their accumulation is controlled by fluctuating water tables during arid climates and conditions of scarce clastic sediment supply (Platt and Wright 1992; Bustillo and Alonza Zarza 2007).

Global trends

The lithologic variability, pedogenic characteristics, and unconformities of the Late Oligocene–Early Pleistocene in the study area, part of the Late Cenozoic-Quaternary strata across the Sahara, may be correlated with brief variations in the global climate and tectonics as well as Sahara development (Fig. 13). Initially accumulation of Katkut Formation during Late Oligocene was formed by north- and northwest-flowing fluvial systems incised into the plateau. The development of these fluvial networks is matched with the eustatic

record and typically colder global climates (Miller et al. 1987, 1991; Zachos et al. 2001; Burke et al. 2003); therefore, an eustatic effect on alluvial sedimentation is proposed here. Several studies (e.g., Garfunkel 1988; Smith et al. 1994; Guiraud et al. 2001; Bosworth and McClay 2001; Thurmond et al. 2004; Bosworth et al. 2005; Lotfy and Van der Voo 2007; Swezey 2009; Abdelkareem et al. 2012) hypothesized that the Sahara during Late Oligocene was located at the current-day latitudes of Chad and Sudan, as a result of Africa's northward drift (Fig. 14a). This geometry favoured conditions for heavy, frequent rainfall (1200–1500 mm/year) (Issawi and Osman 2008) that transported large amounts of coarse-grained fluvial sediments to the Sohag Basin. Besides the humid climatic conditions, regions such as the Red Sea and the Nubian Swell were uplifted and acted as typical sites for their erosion, significant river discharge, and abundance of coarse clastics. This probably explains why Late Oligocene fluvial deposits occur in the study area; these deposits may have formed as a result of this uplift. Issawi and Osman (2008) agree with this interpretation and suggest the northwest-flowing Gilf-fluvial system during the Late Oligocene coincided with an uplift on the southeastern Red Sea margins.

This trend of humidification continued during Late Miocene deposition, as indicated by the dominant fine siliciclastics with lateritic crusts, which were thought to be pedogenic results of strong weathering in humid tropical conditions. Zachos et al. (2001) reported that global warming and humidification occurred during the Late Miocene, creating conditions that were favourable to the deposition of fine siliciclastic material. According to Said (1981), the formation of deep incisions in the Eonile rivers during the late Miocene was caused by the reinforcement of humid conditions during the Mediterranean's drawdown, sometimes referred to as the Messinian crises. Griffin (2002) pointed out that the incision serves as a record of the magnitude of the river systems in Messinian. Notably, many regions of the northern Sahara (e.g., northern Libya, the Chotts Basin of Algeria and Tunisia, and the Quarzazat Basin of Morocco) have Late Miocene humidification with fine siliciclastic facies.

During the Pliocene-Early Pleistocene period, dry conditions prevailed, as the Northern Hemisphere experienced significant global climate shifts, with rising temperatures and a drying trend (Zohans, 2001; Kutzbach et al. 2001; De Schepper et al. 2014; Allstädt et al. 2021). This is evidenced by facies changes, carbonate occurrences, paleosols, and groundwater calcretes in the Pliocene-Early Pleistocene sediments.

In view of the increasing drift of Africa, the trend of aridification in the NE Sahara was formed (Schuster 2006; Swezey 2009; Abdelkareem et al. 2012), and Egypt shifted from a humid subtropical to a northerly dry climate zone. This assumption is confirmed by the proportion of rainfall in the NE Sahara at that time that became less intense (400–600 mm/year) (Issawi and Osman 2008). It is likely that the latitudinal setting of the Sohag Basin during the Pliocene-Early Pleistocene confirmed the arid climate because Egypt was situated roughly between palaeolatitudes 20 and 30° close to the current latitude (Fig. 14b, c).

Additionally, it is likely that the NE African uplifts (Red Sea Mountain chains) and the southward movement of the moisture characters of Asian monsoons could be regarded as important elements driving the evolution of the Late Miocene–Plio-Pleistocene paleoclimate (Rodwell and Hoskins 1996; Griffin 2002; Sepulchre et al. 2006). The humidity in the Late Miocene probably developed in association with the initiation and development of the Asian monsoon. Griffin (2002) mentioned that the Asian monsoon was initiated at about 8–7 Ma and at that time the monsoon transferred moisture mainly to North Africa (Zhisheng et al. 2001). The tropical characters in the study area are attributed to the westward monsoon flow along NE Africa, indicating the Red Sea highlands were reduced in topography during the Late Miocene (Bohannon et al. 1989; Schuster 2006; Sepulchre et al. 2006). The predominance of fine siliciclastic fluvial strata in the Late Miocene sediments confirms their humid character (Fig. 14d).

Recently, Farouk et al. (2022) discussed the astronomical forcing of climate changes in the southeastern Mediterranean Sea during the Early Pliocene. They explained that the alternating sand-shale beds of the Kafr El Sheikh Formation are interpreted as a response to the reflooding at the lower Pliocene rapid sea level rise, which is increasing concurrently with the estimated global average and tropical temperature rise from 5 to 4 Ma, which were evidently influenced by the summer precipitation from the North African monsoon. On the other hand, it is thought that the presence of these moisture characteristics in the sediments of the Nile Delta and their absence in the equivalent sediments in the study area could be interpreted as a result of uplifts of the Red Sea Mountains of NE Africa, which have a significant influence on the direction of monsoons and, consequently, the location of rainfall and moisture. Because of this, the Asian monsoon flow was able to enter the west and produce heavy precipitation in the Nile Delta due to the reduced topography, where the Red Sea highlands are missing. By contrast, in the study area, the Red Sea highlands acted as a topographic barrier and deflected the westward monsoon flow southward along the Red Sea coast (Fig. 14e). During the Late Pliocene–Pleistocene, this phenomenon, which causes monsoons to deflect southward, persisted as topographic barrier blocks. Thus, aridification was continuous throughout the Early Pleistocene (Sepulchre et al. 2006). The uplifts that affected the Red Sea Mountains resulting from rifting processes, reached

a maximum at the Plio-Pleistocene interval (Bothworth 2005; Sepulchre et al. 2006). Furthermore, it is suggested that the southward movement of monsoons contributed significantly to the increased aridity in northeastern Africa in the Pliocene–Pleistocene (Griffin 2002). This movement transformed the humidity in central Africa, southern Asia, and North Africa became drier (Fig. 14f). The occurrence of Early Pleistocene basins that allowed the formation of carbonate lakes along the central and southern Nile courses, west of the Red Sea Mountains, documents such drier climatic conditions (Fig. 14c).

Conclusions

The mixed siliciclastic-carbonate succession in the Sohag Basin records facies changes and pedogenic features, providing information regarding the Late Oligocene to early Pleistocene paleoclimatic trend in the northeastern Sahara. Based on field and sedimentological studies, sixteen lithofacies types of different sedimentary environments have been recognized, which are organized in fluvial and fluvio-lacustrine facies associations. The fluvial association started with conglomerates and sandstones of the Katkut Formation (Late Oligocene) deposited by braided streams, followed upwards by aggrading sandstones and mudstones of the Madamud Formation (Late Miocene-Pliocene) accumulated by channels and flood plains. The fluvio-lacustrine association is represented by breccias and conglomerates of the Issawia Formation which accumulated as alluvial fans that interfingered laterally with the palustrine-lacustrine limestone of the Armant Formation (Early Pleistocene). Pedogenic features including paleosols and calcretes are identified in the fluvial and fluvio-lacustrine facies. Analysis of lithofacies changes and pedogenic characteristics indicates that the paleoclimate of these strata evolved progressively from humid conditions in the Late Oligocene and the Late Miocene to arid conditions by the Pliocene-Early Pleistocene. The evolution of the paleoclimate, therefore, appears to have been influenced by the development of the Asian monsoon and the uplifting of the Red Sea Mountains, in association with the drift of the northern Sahara, where Egypt's paleolatitudinal position moved from a humid tropical-subtropical zone to an arid latitude. This paleoclimate change generated variations in basin sedimentation rates that were controlled by base level and tectonics.

Acknowledgements The author is deeply grateful to Prof. Dr. Abdullah M. Al-Amri (the editor-in-chief) and the anonymous associate editor and reviewers for insightful comments and criticism that improved the manuscript.

Availability of data and materials Data for this research will be made available by the corresponding author upon request.

Declarations

Conflict of interest The author declares that they have no competing interests.

References

Abdelfattah Z (2021) Fluvial architecture of the Upper Cretaceous Nubia Sandstones: an ancient example of sandy braided rivers in central Eastern Desert. Egypt Sed Geol 420:105923

Abdelkareem M, Ghoneim E, El Baz F, Askalany M (2012) New insight on paleoriver development in the Nile basin of the eastern Sahara. J African Earth Sci 62:35–40

Abdelkhalek A, Jonas K, Mohamed H, Ahmed SA (2020).The buried Grand Canyon in Egypt: structural controls on the Neogene River Nile 10.5194/egusphere-egu 2020-821.

Abdelkhalek A, Jonas K (2019) The River Nile rifting in Egypt: a new tectonic model. Geophys Res Abstr 21:1–1

Abdul Aziz H, Sanz-Rubio E, Calvo J, Hilgen F, krijgsman W, (2003) Palaeoenvironmental reconstruction of a Middle Miocene alluvial fan to cyclic shallow lacustrine depositional system in the Calatayud Basin (NE Spain). Sedimentol 50:211–236

Abels HA, Aziz HA, Calvo JP, Tuenters E (2009) Shallow lacustrine carbonate microfacies document orbitally paced lake-level history in the Miocene Teruel Basin (North-East Spain). Sedimentol 56:399–419

Abu Seif S (2015) Geological evolution of Nile Valley, west Sohag, Upper Egypt: a geotechnical perception. Arab J Geosci 8:11049–11072

Adhikari B, Wagreich M (2013) Microfacies analysis and paleoenvironmental significance of palustrine carbonates in the Thakkhola-Mustang Graben (Nepal Himalaya). J Asian Earth Sci 77:117–126

Al Shuaibi A, Khalaf F (2011) Development and lithogenesis of the palustrine and calcrete deposits of the Dibdibba alluvial fan, Kuwait. J of Asian Earth Sci 42:423–439

Alçiçek H, Alçiçek M (2014) Palustrine carbonates and pedogenic calcretes in the Çal basin of SW Anatolia: implications for the Plio-Pleistocene regional climatic pattern in the eastern Mediterranean. CATENA 112:48–55

Alçiçek H, Jimenez-Moreno G (2013) Late Miocene to Plio-Pleistocene fluvio-lacustrine system in the Karacasu Basin (SW Anatolia, Turkey): depositional, paleogeographic and paleoclimatic implications. Sed Geol 291:62–83

Allstädt FJ, Koutsodendris A, Appel E, Rösler W, Reichgelt T, Kaboth-Bahr S, Alexander A, Prokopenko PJ (2021) Late Pliocene to early Pleistocene climate dynamics in western North America based on a new pollen record from paleo-Lake Idaho. Palaeobiodivers Palaeoenviron 101(1):177

Alonso-Zarza AM (2003) Paleoenvironmental significance of palustrine carbonates and calcretes in the geological record. Earth Sci Review 60:261–298

Alonso-Zarza AM, Arenas C (2004) Cenozoic calcretes from the Teruel Graben, Spain: microstructure, stable isotope geochemistry and environmental significance. Sed Geol 167:91–108

Alonso-Zarza A M, Meléndez A, Martín-García R, Herrero M, Martín-Pérez A (2012) Discriminating between tectonism and climate signatures in palustrine deposits: lessons from the Miocene of the Teruel Graben, NE Spain. Earth-Sci Rev 113:41–160

Alonso-Zarza AM, Silva PG (2002) Quaternary laminar calcretes with bee nests: evidences of small scale climatic fluctuations, Eastern Canary Islands, Spain. Paleogeogr Paleoclimat Paleoeco 178:119–135

Alonso-Zarza AM, Tanner LH (2006) Paleoenvironmental record and applications of calcretes and palustrine carbonates. Geol Soc America, Special Paper 416:239

Alonso-Zarza AMC, García J, del Cura M (1992) Palustrine sedimentation and associated features —grainification and pseudo-microkarst—in the Middle Miocene (Intermediate Unit) of the Madrid Basin, Spain. Sed Geol 76:43–61

Alonso-Zarza AM, Genise IF, Verde M (2011) Sedimentology, diagenesis and ichnology of Cretaceous and Palaeogene calcretes and palustrine carbonates from Uruguay. Sed Geol 236:45–61

Alonso-Zarza AM, Wright VP (2010). Palustrine carbonates. In: Alonso-Zarza AM, Tanner LH, editors. Carbonates in continental settings: facies, environments and processes: developments in sedimentology. 1st ed. Elsevier, Amsterdam 61: pp. 225–267.

Arenas C, Pardo G (1999) Latest Oligocene–Late Miocene lacustrine systems of the north-central part of the Ebro Basin (Spain): sedimentary facies model and palaeogeographic synthesis. Palaeogeography, Palaeoclimatology, Palaeoecology 151:127–148

Armenteros I, Huerta P (2006) The role of clastic sediment influx in the formation of calcrete and palustrine facies: a response to paleographic and climatic conditions in the southeastern Tertiary Duero basin (northern Spain). Geol Soci of Amer, Special Paper 416:119–132

Atchley SC, Nordt LC, Dworkin SI (2004) Eustatic control on alluvial sequences stratigraphy: a possible example from the Cretaceous-Tertiary transition of the Tornillo Basin, Big Bend National Park, west Texas, U.S.A. J Sediment Res 74:391–404

Bakeir R, Mahran H (1992) Mineralogical and textural characters of the Pliocene- quaternary nile sediments, wadi Qassab area, Sohag, Egypt. Sohag Pure and Applied. Science. Bulletin Faculty of Science, Egypt 8:215–234

Beilinson E, Veiga G, Spalletti VL (2013) High-resolution sequence stratigraphy and continental environmental evolution: an example from east-central Argentina. Sed Geol 296:21–35

Blair TC, McPhersonb JG (1994) Historical adjustments by Walker River to lake-level fall over a tectonically tilted half-graben floor. Walker Lake Basin, Nevada Sed Geol 92(1–2):7–16

Boggs SJ (2006) Principles of Sedimentology and Stratigraphy, 4th edn. Pearson

Boggs SJ (2009) Petrology of Sedimentary Rocks. Cambridge University Press, New

Bohannon RG, Naeser CW, Schmidt DL, Zimmermann RA (1989) The timing of uplift, volcanism, and rifting peripheral to the Red Sea: a case for passive rifting? J Geophys Res 94(B4):1683–1701

Bosworth W, El-Hawat AS, Helgeson DA, Burke K (2008) Cyrenaican "shock absorber" and associated inversion strain shadow in the collision zone of northeast Africa. Geology 36:695–698

Bosworth W, Huchon Ph, McClay K (2005) The Red Sea and Gulf of Aden Basins. J Afr Earth Sc 43:334–378

Bosworth W, McClay K (2001) Structural and stratigraphic evolution of the Gulf of Suez Rift, Egypt: a synthesis. In: Zeigler, P.A., Cavassa, W., Robertson, A.H.F., Crasquin-Soleau, S. (Eds.), Peri-tethys memoir 6: peri-tethys rift/wrench basins and passive margins. Mémoires du Muséum National d'Histoire

Boulton S, VanDeVelde J, Grimes S (2019) Palaeoenvironmental and tectonic significance of Miocene lacustrine and palustrine carbonates (Aït Kandoula Formation) in the OuarzazateForeland Basin, Morocco. Sed Geol 383:195–215

Bourquin S, Hamouche ER, B, (2010) High-resolution sequence stratigraphy of Upper Triassic succession (Carnian–Rhaetian) of the Zarzaitine outcrops (Algeria): a model of fluvio-lacustrine deposits. J African Earth Sci 58:365–386

Braulta N, Bourquina S, Guillocheaua F, Dabarda M, Bonneta S, Courvillea P, Este´oule-Chouxa J, Stepanoff F, (2004) Mio-Pliocene to Pleistocene paleotopographic evolution of Brittany (France) from a sequence stratigraphic analysis: relative influence of tectonics and climate. Sed Geol 163:175–210

Burke K, MacGregor DS, Cameron NR (2003). Africa's petroleum systems: four tectonic "aces" in the past 600 million years. In: Arthur, T., MacGregor, D.S., Cameron, N.R. (Eds.), Petroleum geology of Africa. Geological Society [London] Special Publication 207: 21–60.

Bustillo M, Alonso-Zarza AM (2007) Overlapping of pedogenesis and meteoric diagenesis in distal alluvial and shallow lacustrine deposits in the Madrid Miocene Basin. Spain Sed Geol 198(3–4):255–271

Cabaleri NG, Benavente CA, Monferran MD, Narváez PL, Volkheimer W, Gallego OF, Do Campo MD (2013) Sedimentology and palaeontology of the upper Jurrasic Puesto Almada Member (Cañadón Asfalto Formation, Fossati sub-basin), Patagonia Argentina: palaeoenvironmental and climatic significance. Sed Geol 296:103–121

Candy I, Black S, Sellwood BW, Rowan JS (2003) Calcrete profile development in Quaternary alluvial sequences, southeast Spain: implications for using calcretes as a basis for landform chronologies. Earth Surf Process Landforms 28:169–185

Chamley, H., 1989.Clay sedimentology. Springer Verlag, Berlin (623 pp.)

De Schepper S, Gibbard P, Salzmann U, Ehlers J (2014) A global synthesis of the marine and terrestrial evidence for glaciation during the Pliocene Epoch. Earth-Sci Rev 135:83–102

Driese SG, Ober EG (2005) Paleopedologic and paleohydrologic records of precipitation seasonally from early Pennsylvanian "underclay" paleosols, USA. J Sediment Res 75(6):997–1010

Dupont-Nivet G, Krijgsman W, Langereis CG, Abels HA, Dai S, Fang X (2007) Tibetan plateau aridification linked to global cooling at the Eocene-Oligocene transition. Nature 445:635–638

El Haddad AA (2007) The impact of paleogeomorphology, local tectonics and paleoclimate on the distribution of the Plio-Pleistocene alluvial and lacustrine sediments of the southern end of Wadi Qena, Eastern Desert, Egypt. M.E.R.C. Ain Shams Univ 21:115–130

El Haddad B (2014) Evolution of the geological history of the Egyptian Nile at Sohag area using sedimentological and studies and remote sensing techniques. Sohag University, Egypt, M Sc

El Deftar T, Issawi B, Abdallah A (1978) Contributions to the geology of Abu Tartur and adjacent areas. Western Desert, Egypt, Ann Geol Survey of Egypt 8:51–90

El Hinnawi M, Abdallah A, Issawi B (1978) Geology of Abu Bayan, Bolaq Stretch, Western Desert. Egypt Ann Geol Survey of Egypt 8:19–50

El Shater A, El Haddad A, El Attar A, Abu GM, Soliman W (2018) Characterization of a Pliocene Egyptian bentonite from Sohag region for pharmaceutical use. Arabian J Geosci 11:385–400

El-Baz F, Maingue M, Robinson CA (2000) Fluvio-aeolian dynamics in the north-eastern Sahara: the relationship between fluvial/Aeolian systems and ground-water concentration. J Arid Environ 44(2):173–183

Eronen JT, Janis CM, Chamberlain CP, Mulch A (2015) Mountain uplift explains differences in Palaeogene patterns of mammalian evolution and extinction between North America and Europe. Proc R Soc Lond B 282:1–8

Esteban M, Klappa CF (1983) Subaerial exposure environment, In: P.A. Scholle et al. (Editors), Carbonate Depositional Environments. Am Assoc Pet Geol. Mem 33:1054

Farouk S, Ren C, Abdeldaim A, Salama A, Wu H, El-Kahtany K, Zaki AS (2022) An astronomical time scale of early Pliocene from

the Mediterranean Sea. Egypt Global and Planetary Change 215:103869. https://doi.org/10.1016/j.gloplacha.2022.103869
Feng Y, Li S, Lu Y (2013) Sequence stratigraphy and architectural variability in late Eocene lacustrine strata of the dongying depression, bohai bay basin, eastern China. Sediment. Geol 295: 1–26
Freytet P, Plaziat JC (1982) Continental carbonate sedimentation and pedogenesis—Late Cretaceous and Early Tertiary of southern France. Contrib to Sedimentology 12:213
Garfunkel Z (1988) Relation between continental rifting and uplifting: evidence from the Suez rift and northern Red Sea. Tectonophysics 150:33–49
Ghazi S, Mountney N (2010) Subsurface lithofacies analysis of the Fluvial Early Permian Warchha Sandstone, Potwar Basin Pakistan. J Geol Soc India 76:505
Ghoneim E, Robinson C, El Baz F (2007) Radar topography data reveal drainage relics in the eastern. Sahara Inter J Remote Sens 28(8):1759–1772
Goudie AS (1983) Calcrete. In: Goudie AS, Pye K (eds) Chemical Sediments and Geomorphology. Academic Press, London, pp 93–131
Griffin DL (2002) Aridity and humidity: two aspects of the late Miocene climate of North Africa and the Mediterranean. Palaeogeogr Palaeoclimatol Palaeoecol 182:65–91
Grimes KG (2012) Surface karst features of the Judbarra, Gregory National Park, Northern Territory, Australia. Helictite 41:15–36
Guiraud R, Issawi B, Bosworth W (2001) Phanerozoic history of Egypt and surrounding areas. In: Zeigler, P.A., Cavassa, W., Robertson, A.H.F., CrasquinSoleau, S. (Eds.), Peri-tethys memoir 6: peritethyan rift/wrench basins and passive margins. Mémoires du Muséum National d'Histoire Naturelle 186: 469–509.
Gürbüz A, Kazancı H, Hakyemez Y, Suzanne A, Leroy G, Neil Roberts G, Ergun Z, Boyraz AS, Esr G, Koç K, Yedek OT, Yücel O (2021) Geological evolution of a tectonic and climatic transition zone: the Beyşehir-Suğla basin, lake district of Turkey. Intl J Earth Sci 110:1077–1107
Gürel A (2017) Geology, mineralogy, and geochemistry of late Miocene paleosol and calcrete in thewestern part of the Central Anatolian Volcanic Province (CAVP), Turkey. Geoderma 302:22–3
Hallan A, Grose J.A, Ruffell A.H (1991). Paleoclimatic significance of changes in clay mineralogy across the Jurassic Cretaceous boundary in England and France.
Haq B U, Hardenbol J, Vail P R (1978) Chronology of fluctuating sea levels since the Triassic. Science 235:1156–1167
Holbrook J, Scott R W, Oboh-Ikuenobe F E (2006) Base-level buffers and buttresses: a model for upstream versus downstream control on fluvial geometry and architecture within sequences. J Sediment Res 76:162–174
Huerta P, Armenteros I (2005) Calcrete and palustrine assemblages on a distal alluvial-floodplain: a response to local subsidence (Miocene of the Duero Basin, Spain). Sed Geol 177:253–270
Huerta P, Armenteros I, Silva P G (2011) Large-scale architecture in non-marine basins: the response to interplay between accommodation space and sediment supply. Sedimentology 58:1716–1736
Issawi B, McCauley J (1993) The Cenozoic landscape of Egypt and its river system. Ann. Geol. Surv. Egypt 19:357–384
Issawi B, Osman R (2008) Egypt during the Cenozoic: geological history of the Nile River. Bull Tethys Geol Soc Cairo 3:43–62
Iwaniw E (1984) Lower Cambrian basin margin deposits in WE Leon, Spain—a model for valley-fill sedimentation in tectonically active, humid climatic setting. Sedimentol 31(1):91–110
Javidan M, Mokhtarpour H, Sahraeyan M, Kheyrandish H (2015) Lithofacies, architectural elements and tectonic provenance of the siliciclastic rocks of the Lower Permian Dorud Formation in the Alborz Mountain Range, Northern Iran. J African Earth Sci 109:211–223
Jo HR, Chough SK (2001) Architectural analysis of fluvial sequences in the northwestern part of Kyongsang Basin (Early Cretaceous), SE Korea. Sed Geol 144:307–334
Jutras P (2017) Climate fluctuations recorded in phreatic and vadose calcretes of the Lower Carboniferous Clyde Sandstone Formation of Machrihanish, Kintyre Peninsula, SW Scotland. J Geol Soc 174(4):646–654
Khadkikar AS, Chamyal LS, Ramesh R (2000) The character and genesis of calcrete in Late Quaternary alluvial deposits, Gujarat, western India, and its bearing on the interpretation of ancient climates. Palaeogeogr Palaeoclimatol Palaeoecol 162:239–261
Khalaf FI, Gaber AS (2008) Occurrence of cyclic palustrine and calcrete deposits within the Lower Pliocene Hagul Formation, East Cairo district. Egypt J African Earth Sci 51:298–312
Khalifa MA, Catuneanu O (2008) Sedimentology of the fluvial and fluvio-marine facies of the Bahariya Formation (Early Cenomanian), Bahariya Oasis, Western Desert Egypt. J African Earth Sci 51:89–103
Kjær KH, Sultan L, Krüger J, Schomacker A (2004) Architecture and sedimentation of outwash fans in front of the Myrdalsjökull ice cap, Iceland. Sed Geol 172:139–163
Kraus MJ (1999) Paleosols in clastic sedimentary rocks: their geologic applications. Earth Sci Rev 47:41–70
Kraus MG, Hasiotis ST (2006) Significance of different modes of rhizolith preservation to interpreting paleoenvironmental and paleohydrologic settings: examples from Paleogene paleosols, Bighorn Basin, Wyoming, USA. J Sediment Res 76(4):633–646
Kraus MJ, Aslan A (1999) Paleosol sequence in floodplain environments: a hierarchical approach. In: Thiry M, Simon-Coincon R (eds) Palaeo-weathering, palaeo-surfaces and related continental deposits. International Association of Sedimentologists Special Publication, vol 27 303–321.
Kutzbach JE, Prell WL, Porter SC (2001) Evolution of Asian monsoons and phased uplift of the Himalaya-Tibetan plateau since Late Miocene times. Nature 411:62–66
Lansbery, L (2011). Geological and geomorphological evolution of the Egyptian Nile between Asswan and Kom Ombo: a remote sensing and field study approach., Msc. Missouri University of Science and Technology, Rolla, MO. p. 83.
Lindbo DL, Stolt MH, Vepraskas MJ (2010) Redoximorphic features. In: Stoops G, Marcelino V, Mees F (eds) Interpretation of micromorphological features of soils and regoliths. Elsevier, Amsterdam, pp 129–147
Lotfy H, Van der Voo R (2007) Tropical northeast Africa in middle–late Eocene: paleomagnetism of the marine-mammals sites and basalts in Fayum province. Egypt J African Earth Sci 47:135–152
Mack G, James W, Monger H (1993) Classification of paleosols. Geol Soc Am Bull 105:129–136
Mack G, Cole DR, Treviño L (2000) The distribution and discrimination of shallow, authigenic carbonate in the Pliocene-Pleistocene Palomas basin, southern Rio Grande rift. Geolo Soci of America Bulletin 112:643–656
Mahran T, Hassan A (2019) Alluvial karstification and paleodoline development in Eocene limestones, a case study from west Sohag City, Egypt: implications for causes and impacts. Arab J Geosci 12:240
Mahran T, Hassan A (2023) Controls on Late Miocene to Early Quaternary continental sedimentation during the development of the Sohag basin, Nile Valley Egypt. J Afr Earth Sci 199:104829
Miall AD (1977) A review of the braided river depositional environment. Earth-Sci Rev 13:1–62
Miall AD (1996) The geology of fluvial deposits: sedimentary facies, basin analysis and petroleum geology. Springer-Verlag, Berlin, p 582

Miall AD (1978) Lithofacies types and vertical profile models in braided river deposits: a summary. In: Miall, A.D. (Ed.), Fluvial Sedimentol-ogy. Canadian Society of Petroleum Geology Memoir 5: 597–604.

Miall AD (2010). Alluvial deposits. In: James NP, Daruymble RW editors. Facies models. Geol Association Canada 6: 105–137.

Miguel Nieto-Albert N, Molina J M, Molina PA, Ruiz-Ortiz PA 2022. Palustrine sediments between two isolated shallow carbonate platforms (Aptian–Albian Transition, Prebetic of Jaén, South Spain). Minerals 12(2):116; https://doi.org/10.3390/min12020116

Miller KG, Fairbanks RG, Mountain GS (1987) Tertiary oxygen isotope synthesis, sea level history, and continental margin erosion. Paleoceanography 2:1–19

Miller KG, Wright JD, Fairbanks RG (1991) Unlocking the ice house: Oligocene-Miocene oxygen isotopes, eustasy, and margin erosion. J Geophys Res 96(B4):6829–6848

Nador A, Thamo-Boaso E, Magyari A, Babinszk E (2007) Fluvial response to tectonic and climatic change during Late Weichselian in the eastern part of the Pannonian Basin (Hungary). Sediment Geology 202:174–192

Netterberg F (1980) Geology of southern African calcretes, 1. Terminology, description, macrofeatures, and classification. Trans Geol Soc S Afr 83:255–283

Olsen H (1988) The architecture of a sandy braided-meandering river system: an example from the Lower Triassic Solling Formation (M. Buntsandstein) in W Germany. Geol Rundsch 77:797–814

Paula-Freitas A. (2010) Analise Estratigrafica do IntervaloSiliciclastico Aptiano da Bacia do Araripe (Formacao Rio da Batateira). MSc Thesis. Universidade Federal do Rio Janeiro, Rio de Janeiro, Brazil.

Philobbos E, Riad S, Omran A, Othman A (2000) Stages of fracture development controlling the evaluation of the Nile Valley in Egypt. Egypt J Geol 127:31–46

Picford M, Wanas H, Mein P, Soliman H (2008) Humid conditions in the Western Desert of Egypt during the Vahesian (Late Miocene). Bull Tethys Geol Soc Cairo 3:63–79

Pla-Pueyo S, Gierlowski-Kordesch E, Viseras C, Soria J (2009) Major controls on sedimentation during the evolution of a continental basin: Pliocene-Pleistocene of the Guadix Basin (Betic Cordillera, southern Spain). Sediment Geol 219:97–114

Platt NH, Wright VP (1992) Palustrine carbonates at the Florida Everglades: towards an exposure index for the fresh-water environment. J Sediment Petrol 62:1058–1071

Ramstein G, Fluteau F, Besse J, Joussaume S (1997). Effect of orogeny, plate motion and land–sea distribution on Eurasian climate change over the past 30 million years.

Retallack GJ, Alonso-Zarza AM (1998) Middle Triassic paleosols and paleoclimate of Antarctica. J Sediment Res 68:169–184

Retallack GJ (2008) Cambrian paleosols and landscapes of South Australia. Aust J Earth Sci 55:1083–1106

Retallack G (2001) Soils of the past; an introduction to paleopedology, 2nd edn. Blackwell Science, Oxford, p 404

Righi D, Meunier A (1995).Origin of clays by rock weathering and soil formation. In: Robinson C, El-Baz F, Ozdogan M, Ledwith M, Blanco D, Oakley S, lnzana J (2000). Use of radar data to delineate palaeodrainage flow directions in the Selima sand sheet, eastern Sahara. Photogramm Eng Remote Sens 66 (6):745–753.

Robinson CA, El-Baz F, Ozdogan M, Ledwith M, Blanco D, Oakley S, Inzana J (2000) Use of radar data to delineate paleodrainage flow direction in the Selima sand sheet, Eastern Sahara. Photogrammetric Engineering and Remote Sensing 66:745–753

Ruffell A, McKinley JM, Worden RH (2002) Europe comparison of clay mineral stratigraphy to other proxy palaeoclimate indicators in the Mesozoic of NW Europe. Philos Trans Royal Soc London A 360:675–693

Sahraeyan M (2013) Sedimentology and palaeogeography of conglomerates from the Aghajari Formation in Zagros Basin, SW Iran. Intl J Adv Geosci 1(1):13–22

Sahraeyan M, Bahrami M (2012) Petrography and provenance of sandstones from the Aghajari Formation, Folded Zagros Zone, southwestern Iran". Intl J Basic Appl Sci 1(3):283–298

Said R (1981) The geological evolution of the river Nile. Springer, New York, Heidelberg, Berlin, p 146

Said R (1990). The geology of Egypt: Balkema AA, Rotterdam, Brookfield, 734 pp.

Sakran S, Shehatab A, Osman O, El-Sherbiny M (2019) Superposed tectonic regimes in west Beni Suef basin, Nile Valley, Egypt: implications to source rock maturation and hydrocarbon entrapment. J Afr Earth Sc 154:1–19

Sanz M, Alonso-Zarza AM, Calvo J (1995) Carbonate pond deposits related to semi-arid alluvial systems: examples from the Tertiary Madrid Basin. Spain Sediment 42:437–452

Scherer C, Goldberg K, Bardola T (2015) Facies architecture and sequence stratigraphy of an early post-rift fluvial succession, Aptian Barbalha Formation, Araripe Basin, northeastern Brazil. Sediment Geol 322:43–62

Schuster M, Duringer P, Ghienne J-F, Vignaud P, Mackaye HT, Likius A, Brunet M (2006) The age of the Sahara Desert. Science 311:821

Selley RC (1982) An introduction into sedimentology. Academic, New York, p 408p

Sepulchre P, Ramstein G, Fluteau F, Schuster M, Tiercelin J, Brunet M (2006) Tectonic uplift and Eastern Africa aridification. Science 313:1419–1423

Sheldon N, Tabor N (2009) Quantitative paleoenvironmental and paleoclimatic reconstruction using paleosols. Earth Sci Rev 95:1–52

Sim L, Chambers J, Davis J (2006) Ecological regime shifts in salinised wetland systems. I. Salinity thresholds for the loss of submerged macrophytes. Hydrobiologia 573:89–107

Smith A, Smith DG, Funnell B (1994) Atlas of Mesozoic and Cenozoic coastlines. Cambridge University Press, Cambridge, UK, p 99

Soreghan GS, Soreghan MJ, Sweet DE, More KD (2009) Hot fan or cold outwash? Hypothesized proglacial deposition in the Upper Paleozoic Cutler Formation, western tropical Pangea. J Sediment Res 79:495–522

Swezey C (2009) Cenozoic stratigraphy of the Sahara, Northern Africa. J African Earth Sci 53:89–121

Tanner LH (2000) Palustrine-lacustrine and alluvial facies of the (Norian) Owl Rock Formation (Chinle Group), Four Corners Region, southwestern U.S.A implications for Late Triassic paleoclimate. J of Sediment Research 70:1280–1289

Tanner LH, Lacus SG (2012) Carbonate facies of the Upper Triassic Ojo Huelos Member, San Pedro Arroyo Formation (Chinle Group), southern New Mexico: paleoclimatic implications. Sediment Geol 273–274:73–90

Tanner LH, Lucas SG (2018) Pedogenic record of climate change across the Pennsylvanian-Permian boundary in Red-bed strata of the Cutler Group, northern New Mexico, USA. Sediment Geol 373:98–110

Tanner LH, Lucas SG (2006). Calcareous paleosols of the Upper Triassic Chinle Group, Four Corners region, southwestern United States: climatic implications, in Alonso-Zarza AM and Tanner LH, eds., Paleoenvironmental record and applications of calcretes and palustrine carbonates. Geological Society of America Special Paper 416: 53–74.

Thiry M (2000) Palaeoclimatic interpretation of clay minerals in marine deposits: an outlook from the continental origin. Earth-Sci Rev 49(1–4):201–221

Thurmond A, Stern R, Abdelsalam M, Abdeen M, Hinz E (2004) The Nubian Swell. J African Earth Sci 39:401–407

Tuner P (1980): Continental red beds. Developments in Sedimentology 29, Elsevier, Amsterdam (562).
Türkmen A, Aksoy E, Taogin C (2007) Alluvial and lacustrine facies in an extensional basin: the Miocene of Malatya basin, eastern Turkey. J Asian Earth Sci 30:181–198
Wanas H, Sallam E (2014) Calcretes and palustrine carbonates in the Oligo-Miocene clastic–carbonate unit of the Farafra Oasis, Western Desert, Egypt: their origin and paleoenvironmental significance. J African Earth Sci 95:145–154
Wanas H, Sallam E, Zobaa M, Li X (2015) Mid-Eocene alluvial-lacustrine succession at Gebel El–Goza El-Hamra (Shabrawet area, NE Eastern Desert, Egypt): facies analysis sequence stratigraphy and paleoclimatic implications. Sediment Geol 329:115–129
Wright VP, Tucker ME (1991) Calcretes: An introduction, inWright, V.P., and Tucker, M.E., eds., Calcretes: New York, Blackwell Scientific 1–22
Wright V (1999). Assessing flood duration gradients and fine-scale environmental change on ancient floodplains. In: Marriott SB, Alexander J (Eds.), Floodplains: interdisciplinary approaches: Geological Society, London, Special Publication 163: 279–287.
Youssef MM (2003) Structural Setting of Central and South Egypt: an Overview Micropaleontology 49(1):1–13
Zachos J, Pagani M, Sloan L, Thomas E, Billups K (2001) Trends, rhythms, and aberrations in global climate 65 Ma to present. Science 292:686–693
Zachos J, Pagani M, Sloan L, Thomas E, Billups K (2001) Trends, rhythms, and abberations in global climate 65 Ma to present. Science 292:686–693
Zhisheng An, Kutzbach J, Prell W, Porter S (2001) Evolution of Asian monsoons and phased uplift of the Himalaya-Tibetan plateau since Late Miocene. Nature 411:62–66